Preprints.org

Article

Not peer-reviewed version

Wide and Ultrawide Bandgap Power Semiconductors: A Comprehensive System-Level Review

Giuseppe Galioto , Gianpaolo Vitale * , Antonino Sferlazza , Giuseppe Lullo , Giuseppe Costantino Giaconia

Posted Date: 29 January 2026

doi: 10.20944/preprints202601.2280.v1

Keywords: efficiency; gallium nitride (GaN); power density; silicon carbide (SiC); wide-bandgap (WBG); ultrawide-bandgap (UWBG); power electronics; electric vehicles; EMI mitigation; vertical GaN; bidirectional switch (BDS); systematic review; PRISMA methodology

Preprints.org is a free multidisciplinary platform providing preprint service that is dedicated to making early versions of research outputs permanently available and citable. Preprints posted at Preprints.org appear in Web of Science, Crossref, Google Scholar, Scilit, Europe PMC.

Copyright: This open access article is published under a Creative Commons CC BY 4.0 license, which permit the free download, distribution, and reuse, provided that the author and preprint are cited in any reuse.

Preprints.org (www.preprints.org) | NOT PEER-REVIEWED | Posted: 29 January 2026 doi:10.20944/preprints202601.2280.v1

Disclaimer/Publisher's Note: The statements, opinions, and data contained in all publications are solely those of the individual author(s) and contributor(s) and not of MDPI and/or the editor(s). MDPI and/or the editor(s) disclaim responsibility for any injury to people or property resulting from any ideas, methods, instructions, or products referred to in the content.

Article

Wide and Ultrawide Bandgap Power Semiconductors: A Comprehensive System-Level Review

Giuseppe Galioto [1], Gianpaolo Vitale [2,*], Antonino Sferlazza [1], Giuseppe Lullo [1] and Giuseppe Costantino Giaconia [1]

[1] Department of Engineering, University of Palermo, Viale delle Scienze, Building 9, 90128 Palermo, Italy
[2] Institute for High Performance Computing and Networking (ICAR), National Research Council of Italy, Via Ugo La Malfa 153, 90146 Palermo, Italy
* Correspondence: gianpaolo.vitale@icar.cnr.it

Abstract

This review analyzes the transition from silicon to wide-bandgap (WBG) and ultrawide-bandgap (UWBG) semiconductor materials for power electronics, focusing on Silicon Carbide (SiC) and Gallium Nitride (GaN) technologies. Following a PRISMA-based systematic review methodology, we analyzed 116 peer-reviewed publications spanning device technology, converter architectures, and system applications. We employ a bottom-up approach, progressing from fundamental material properties through device architectures and converter topologies to system-level implications. We examine how intrinsic material properties enable operation at elevated temperatures, voltages, and frequencies while minimizing losses. Through analysis of Figures of Merit and system-level Key Performance Indicators, we quantify WBG benefits across automotive, industrial, renewable energy, and consumer electronics sectors, demonstrating 3–5x power density improvements and 20–40% cost reductions. The review presents emerging device technologies including vertical GaN for medium-voltage applications and monolithic bidirectional switches (BDS) enabling single-stage power conversion. We provide the first comprehensive topology-level comparison of emerging vertical GaN and monolithic bidirectional switches against established SiC solutions, identifying specific applications where each technology offers advantages. A comprehensive topology-by-topology comparison between SiC and GaN is provided, offering design guidelines for device selection. The review addresses practical constraints including dynamic on-resistance degradation, threshold voltage instability, and electromagnetic interference challenges for both SiC and GaN. Finally, we examine emerging UWBG materials (beta-Ga2O3, AlN, c-BN, Diamond) and their development status, manufacturing challenges, supply chain considerations, and commercialization prospects for ultra-high-voltage applications.

Keywords: efficiency; gallium nitride (GaN); power density; silicon carbide (SiC); wide-bandgap (WBG); ultrawide-bandgap (UWBG); power electronics; electric vehicles; EMI mitigation; vertical GaN; bidirectional switch (BDS); systematic review; PRISMA methodology

---

1. Introduction

The global power electronics sector is experiencing a transformative shift driven by increasingly stringent demands for sustainable energy systems, improved operational efficiency, and reduced carbon emissions. In 2023, energy-related carbon dioxide (CO_2) emissions reached approximately 37.4 Gt, representing an increase of roughly 1.1% compared to 2022 [1]. Although the adoption of clean energy technologies—including solar photovoltaics, wind power, and electric vehicles—has tempered the rate of emissions growth, these persistently high emission levels underscore that incremental improvements alone are insufficient; substantial efficiency gains across the entire energy conversion chain are essential [2].

© 2025 by the author(s). Distributed under a Creative Commons CC BY license.

Figure 1 illustrates the historical trend of global carbon dioxide emissions from energy and industrial sources (1970–2023), highlighting the urgency of reducing emissions growth through more efficient power conversion technologies.

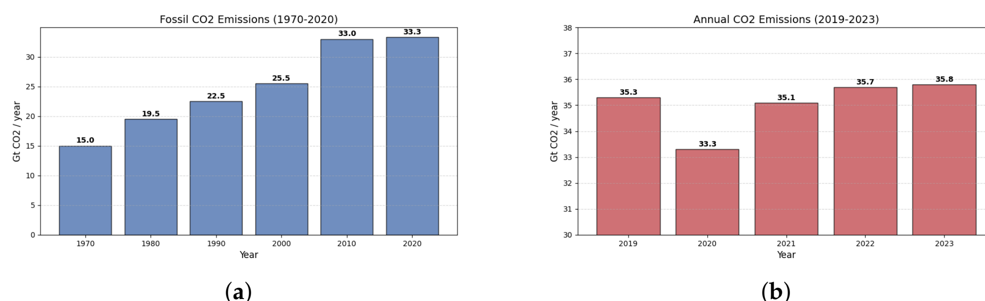

(a) (b)

Figure 1. Global energy-related and industrial CO_2 emissions (1970–2023). a) CO_2 Emissions in last 40 years, b) CO_2 Emissions in last 5 years. Data arranged from: Liu et al. [2].

Central to addressing this challenge is the transition from traditional silicon-based power semiconductors to wide-bandgap (WBG) and ultrawide-bandgap (UWBG) materials, most notably Silicon Carbide (SiC) and Gallium Nitride (GaN) [3,4]. This technological evolution represents far more than a simple material substitution; it constitutes a paradigm shift in power conversion capability that enables revolutionary improvements in efficiency, power density, and thermal performance across virtually all application domains [5–7].

Figure 2 illustrates the cascading benefits of improved power electronics efficiency across different application sectors, demonstrating how WBG technology contributes to overall system sustainability through environmental, economic, and technical improvements.

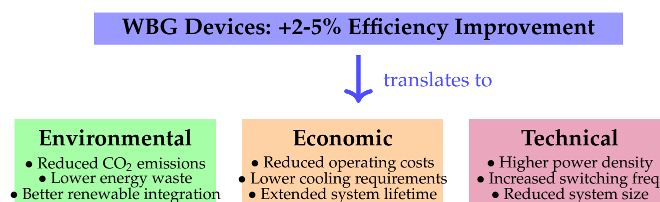

Figure 2. Key benefits of WBG technology across different application sectors

Power converters based on semiconductor switching devices regulate energy flow in nearly every modern electrical system, from renewable energy installations and electric vehicle drivetrains to industrial motor drives and data center infrastructure. Even modest improvements in converter efficiency—on the order of 2–5%—can yield substantial reductions in overall energy consumption and associated emissions when deployed at scale [8,9]. The cascading benefits of WBG technology extend beyond raw efficiency improvements to encompass reduced cooling requirements, smaller passive components, and enhanced system reliability.

The economic case for WBG adoption is equally compelling. In large-scale facilities such as data centers operating 10 MW of server power supplies, improving efficiency from 94% to 97% can result in annual energy savings exceeding $450k [10]. For electric vehicles, a 3% efficiency improvement in the traction inverter translates to approximately 20 km of additional driving range per charge, directly enhancing user experience while reducing battery degradation and total cost of ownership [11,12].

This review paper provides a comprehensive analysis of the current state and future prospects of WBG and UWBG power semiconductors using a bottom-up approach. Section 2 presents fundamental material properties and comparative analysis through various figures of merit. Section 3 provides an in-depth analysis of emerging UWBG materials including their development status and commercialization timeline. Section 4 analyzes SiC and GaN device configurations. Section 5 addresses converter

© 2025 by the author(s). Distributed under a Creative Commons CC BY license.

Preprints.org (www.preprints.org) | NOT PEER-REVIEWED | Posted: 29 January 2026
doi:10.20944/preprints202601.2280.v1

topologies for both SiC and GaN devices. Section 6 provides a comprehensive SiC vs. GaN comparison including gate driver requirements. Section 7 discusses system-level implications and quantifies benefits across multiple performance dimensions. Section 8 examines the application landscape with detailed case studies. Section 9 covers reliability considerations and practical constraints for SiC and GaN. Finally, Section 10 provides conclusions and future research directions. The list of acronyms is provided at the end of the document.

1.1. Literature Review Methodology

This review follows a systematic approach adapted from the PRISMA (Preferred Reporting Items for Systematic Reviews and Meta-Analyses) guidelines to ensure transparency, reproducibility, and comprehensiveness in the literature selection process [13].

1.1.1. Search Strategy and Databases

The literature search was conducted across multiple academic databases including IEEE Xplore, ScienceDirect, Web of Science, Scopus, and Google Scholar. The search period covered publications from January 2014 to December 2025, capturing the critical decade of WBG commercialization and maturation. The primary search keywords and Boolean combinations employed were:

- Primary keywords: "wide bandgap semiconductors", "silicon carbide power devices", "gallium nitride HEMT", "SiC MOSFET", "GaN power electronics"
- Secondary keywords: "ultrawide bandgap", "power converter topology", "electric vehicle inverter", "DC-DC converter", "gate driver design"
- Emerging technology keywords: "vertical GaN", "bidirectional switch", "gallium oxide power", "diamond semiconductor", "aluminum nitride"
- Application keywords: "traction inverter", "on-board charger", "solar inverter", "data center power supply"

Boolean combinations such as ("SiC" OR "GaN") AND ("power converter" OR "inverter" OR "DC-DC") AND ("efficiency" OR "power density" OR "switching frequency") were employed to capture the intersection of device technology and converter applications.

1.1.2. Screening and Selection Process

Figure 3 presents the PRISMA flow diagram illustrating the systematic literature selection process.

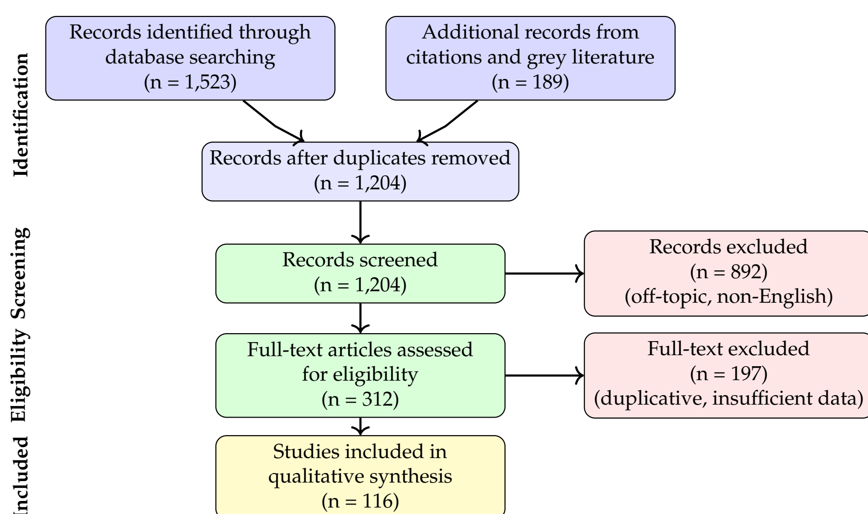

Figure 3. PRISMA flow diagram for systematic literature selection process.

Table 1 summarizes the distribution of selected literature by category.

© 2025 by the author(s). Distributed under a Creative Commons CC BY license.

Preprints.org (www.preprints.org) | NOT PEER-REVIEWED | Posted: 29 January 2026
doi:10.20944/preprints202601.2280.v1

Table 1. Distribution of Reviewed Literature by Category.

Category	Papers Reviewed	Key Focus Areas
SiC Device Technology	22	MOSFET structures, reliability, gate oxide
GaN HEMT Technology	26	E-mode/D-mode, dynamic R_{on}, cascode
Converter Topologies	19	DAB, buck, inverters, PFC
System Applications	20	EV, solar, data center, industrial, hydrogen
UWBG Materials	17	Ga_2O_3, AlN, Diamond, c-BN
EMI & Gate Drivers	9	dv/dt control, layout, filtering
Emerging Technologies	3	Vertical GaN, BDS, monolithic integration
Total	**116**	—

1.1.3. Inclusion and Exclusion Criteria

Studies were included if they: (1) presented original research or comprehensive reviews on WBG/UWBG power semiconductor devices; (2) provided quantitative data on device performance, converter efficiency, or system-level benefits; (3) were published in peer-reviewed journals or major IEEE conference proceedings; (4) addressed practical implementation aspects including reliability, EMI, or thermal management.

Studies were excluded if they: (1) focused exclusively on RF/microwave applications without power electronics relevance; (2) presented only simulation results without experimental validation; (3) were superseded by more comprehensive studies from the same research group; (4) lacked quantitative performance metrics for comparison.

1.2. Comparison with Existing Review Literature and Added Value

Table 2 presents a systematic comparison between this review and recent similar publications, highlighting the unique contributions and gaps addressed by this work.

Table 2. Comparison with Recent WBG Semiconductor Review Papers.

Review Paper	Year	Scope	Strengths	Limitations
Buffolo et al. [8]	2024	Industrial SiC/GaN devices	Excellent reliability analysis; commercial device survey	Limited topology comparison; no UWBG coverage
Rafin et al. [14]	2023	WBG/UWBG overview	Broad material coverage; historical context	Limited system-level analysis; no vertical GaN/BDS
Nature Reviews [15]	2025	Carbon neutrality focus	Sustainability perspective; policy implications	Limited converter topology detail
Kumar et al. [16]	2022	Material properties	Comprehensive FOM analysis	Dated commercial landscape; no emerging devices
She et al. [17]	2014	HVDC applications	Deep HVDC analysis	Pre-dates GaN maturation
This Review	**2025**	**System-level WBG/UWBG**	**See Added Value below**	—

The work by Wu et al. [18] was considered as not concurrent in this review and it was included as reference in Section 6.4.2.

1.2.1. Unique Contributions and Added Value

This review addresses several critical gaps in the existing literature:

(1) Comprehensive Topology-by-Topology SiC vs. GaN Comparison: Unlike previous reviews that focus primarily on device-level characteristics, this work provides detailed design guidelines for device selection across all major converter topologies (Table 8), enabling practicing engineers to make informed technology choices based on specific application requirements.

© 2025 by the author(s). Distributed under a Creative Commons CC BY license.

(2) Emerging Device Technologies: This review provides the first comprehensive coverage of vertical GaN power devices and monolithic bidirectional switches (BDS) in the context of converter topologies. While Buffolo et al. [8] acknowledge these technologies, our work provides detailed analysis of their impact on specific topologies including matrix converters, Vienna rectifiers, and current-source inverters.

(3) Updated UWBG Materials Assessment: The UWBG section (Section 3) incorporates the latest developments through 2025, including the 7.3 MV/cm AlN breakthrough [19], the 4.6 kV diamond SBD demonstration [20], and the first n-channel diamond MOSFET [21]. Previous reviews [3,16] lack these recent milestones.

(4) Bottom-Up Systematic Approach: This review uniquely employs a bottom-up methodology (Materials → Devices → Converters → Systems), providing clear traceability from fundamental material properties through figures of merit to system-level KPIs. This approach enables readers to understand *why* specific devices excel in particular applications.

(5) Quantitative System-Level Benefits: Section 7 provides quantified economic analysis with payback periods for each application sector—data largely absent from device-focused reviews.

(6) Practical Design Constraints: The review addresses real-world implementation challenges including dynamic R_{on} degradation mechanisms, threshold voltage instability, and gate driver optimization requirements (Table 9) that are often overlooked in material-focused surveys.

1.2.2. Research Gap Analysis

Figure 4 illustrates the positioning of this review relative to existing literature across two key dimensions: device technology depth and system integration scope.

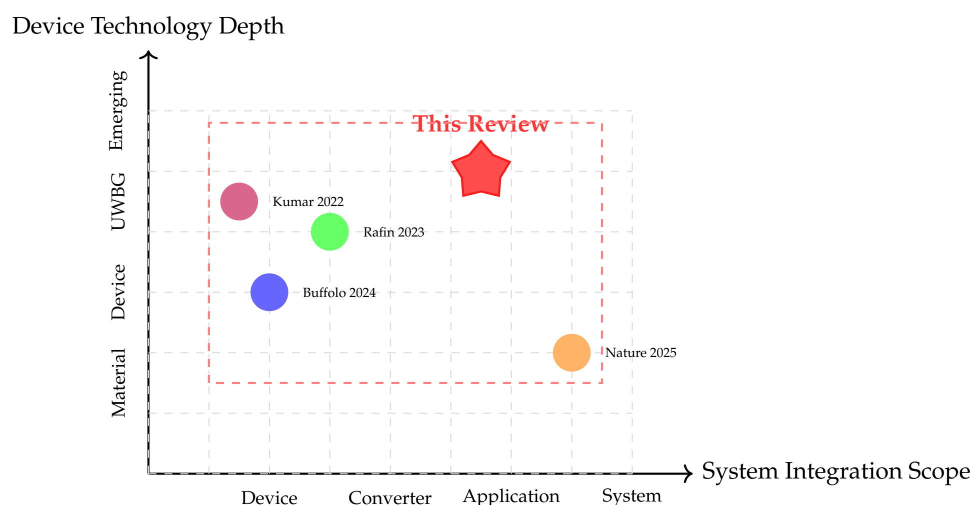

Figure 4. Positioning of this review relative to existing WBG literature. This work uniquely spans from fundamental device technology through system-level integration while incorporating emerging technologies.

2. Material Properties and Comparative Analysis

The fundamental material properties of semiconductors determine the ultimate performance limits achievable in power electronic devices. WBG and UWBG materials demonstrate exceptional versatility across power electronics and Radio Frequency (RF) applications due to their capacity to operate reliably in high-temperature and harsh environments [4,16].

2.1. Intrinsic Material Characteristics

Table 3 summarizes the key properties of silicon alongside WBG materials (4H-SiC, GaN) and emerging UWBG materials (β-Ga_2O_3, AlN, c-BN, Diamond).

© 2025 by the author(s). Distributed under a Creative Commons CC BY license.

Preprints.org (www.preprints.org) | NOT PEER-REVIEWED | Posted: 29 January 2026 doi:10.20944/preprints202601.2280.v1

Table 3. Material Properties of Semiconductors for Power Electronics, data taken from [3].

Parameter	Si	4H-SiC	GaN	β-Ga_2O_3	AlN	c-BN	Diamond
E_g (eV)	1.12	3.23	3.4	4.9	6.2	6.4	5.5
E_c (MV/cm)	0.3	2.5	3.3	8	15	12	10
μ_n (cm^2/Vs)	1440	950	2000	250	850	200	4500
v_{sat} (10^7 cm/s)	1.0	2.0	2.4	1.1	1.4	2.0	2.3
κ (W/cm·K)	1.5	3.7	2.5	0.1–0.3	2.85	13	23

Figure 5 provides a comprehensive radar chart comparison between silicon and U/WBG devices across multiple key parameters, visually demonstrating the performance advantages of advanced semiconductor materials.

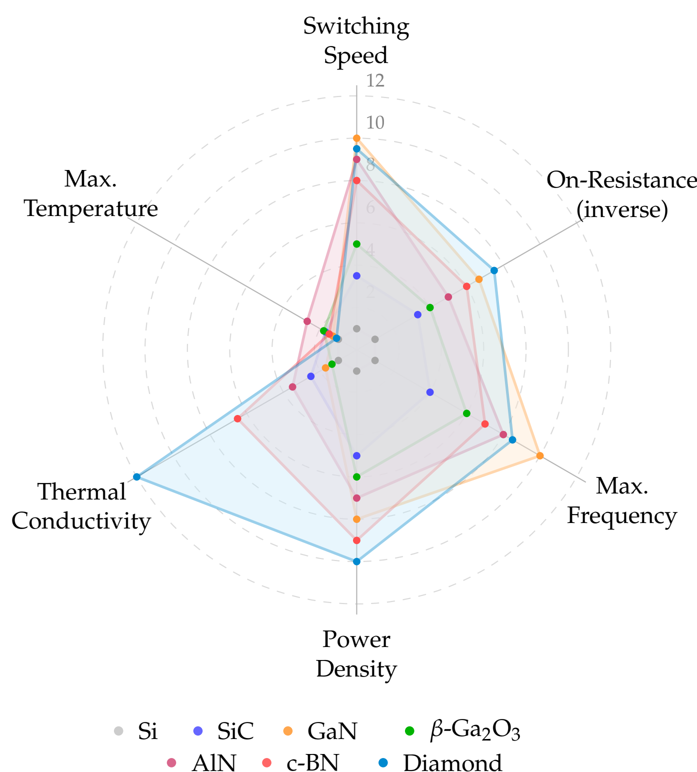

Figure 5. Radar chart comparison of power semiconductor materials. Normalized performance relative to Si (adapted from [3,4]).

The bandgap energy E_g represents the energy required to excite an electron from the valence band to the conduction band. Materials with larger bandgaps exhibit higher intrinsic breakdown voltages and can operate at elevated temperatures without excessive thermally-generated leakage current [5]. The wide bandgap of SiC (3.23 eV) and GaN (3.4 eV) compared to silicon (1.12 eV) fundamentally enables operation at higher voltages and temperatures.

The critical electric field E_c defines the maximum electric field a material can sustain before avalanche breakdown occurs [17]. SiC and GaN exhibit critical fields approximately 8–11× higher than silicon, while UWBG materials such as β-Ga_2O_3 and AlN approach 30–50× improvement.

Electron mobility μ_n quantifies how rapidly charge carriers drift through the material under an applied electric field [22]. While SiC exhibits somewhat lower mobility than silicon (950 vs. 1440 cm^2/Vs), GaN offers superior mobility (2000 cm^2/Vs), and diamond presents exceptional mobility (4500 cm^2/Vs) for future applications.

© 2025 by the author(s). Distributed under a Creative Commons CC BY license.

Preprints.org (www.preprints.org) | NOT PEER-REVIEWED | Posted: 29 January 2026 doi:10.20944/preprints202601.2280.v1

Thermal conductivity κ governs the ability to conduct heat away from active device regions, critically impacting power handling capability and long-term reliability [23]. SiC's thermal conductivity (3.7 W/cm · K) substantially exceeds that of silicon (1.5 W/cm · K), while diamond's exceptional value (23 W/cm · K) positions it as the ultimate material for extreme power density applications.

2.2. *Quantitative Performance Metrics: Figures of Merit*

Several Figures of Merit (FOMs) have been developed to enable quantitative comparison of semiconductor technologies [24–27].

Baliga's Figure of Merit (BFOM) characterizes the trade-off between on-resistance and breakdown voltage for unipolar power devices [24]:

$$\text{BFOM} = \frac{\varepsilon_r \mu_n E_c^3}{4} \tag{1}$$

Baliga High-Frequency Figure of Merit (BHFFOM) accounts for switching losses [28]:

$$\text{BHFFOM} = \frac{\mu_n E_c^2}{2\pi} \tag{2}$$

Johnson's Figure of Merit (JFOM) characterizes the maximum power-frequency product [25]:

$$\text{JFOM} = \left(\frac{v_{sat} E_c}{2\pi}\right)^2 \tag{3}$$

Keyes' Figure of Merit (KFOM) evaluates thermal management and power density limits [26]:

$$\text{KFOM} = \frac{\kappa \cdot v_{sat}}{4\pi\varepsilon_0\varepsilon_r} \tag{4}$$

Combined High-Frequency Figure of Merit (CHFFOM) extends BHFFOM to include thermal effects [27]:

$$\text{CHFFOM} = \kappa \cdot \text{BHFFOM} = \frac{\kappa \mu_n E_c^2}{2\pi} \tag{5}$$

Thermal Figure of Merit (TFOM) [29] specifically addresses heat dissipation capability:

$$\text{TFOM} = \frac{\lambda}{k_B T} \tag{6}$$

where k_B is Boltzmann's constant and T is absolute temperature.

Table 4 presents normalized FOM values relative to silicon.

Table 4. Normalized Figures of Merit for Power Semiconductor Materials (Si = 1) data taken from [3,24,27].

Material	BFOM	BHFFOM	JFOM	KFOM	CHFFOM	TFOM
Si	1	1	1	1	1	1
4H-SiC	317	13.7	20	4.8	29	3.3
GaN	846	27.5	33	1.4	56	2.2
β-Ga_2O_3	3444	10.5	14	0.9	30	0.8
AlN	3360	57.6	68	13.8	562	9.2
Diamond	50000	81.2	163	46.2	2114	33

3. Emerging UWBG Materials: Development Status and Commercialization

While SiC and GaN technologies have achieved commercial maturity, ultrawide-bandgap (UWBG) materials represent the next frontier in power semiconductor development. These materials, characterized by bandgaps exceeding 4 eV, offer theoretical performance advantages that could enable applications beyond the capabilities of current WBG devices [3].

© 2025 by the author(s). Distributed under a Creative Commons CC BY license.

Preprints.org (www.preprints.org) | NOT PEER-REVIEWED | Posted: 29 January 2026 doi:10.20944/preprints202601.2280.v1

3.1. Beta-Gallium Oxide (β-Ga_2O_3)

β-Ga_2O_3 has emerged as one of the most promising UWBG materials due to its unique combination of properties and manufacturing advantages [30]. With a bandgap of 4.9 eV and a critical electric field of 8 MV/cm, β-Ga_2O_3 exhibits a Baliga Figure of Merit (BFOM) more than 3000$\times$ that of silicon, suggesting tremendous potential for high-voltage power devices.

A key advantage of β-Ga_2O_3 is its compatibility with melt-growth techniques including the Floating Zone (FZ), Czochralski (CZ), and Edge-defined Film-fed Growth (EFG) methods. These methods enable production of large-diameter, high-quality single-crystal substrates at potentially lower costs than the vapor-phase growth required for SiC and GaN substrates. Currently, 2-inch and 4-inch β-Ga_2O_3 substrates are commercially available, with 6-inch substrates demonstrated in research laboratories [31].

Significant device milestones have been achieved in recent years. Researchers at the Korea Electronics and Telecommunications Research Institute (ETRI) demonstrated 3 kV-class β-Ga_2O_3 MOSFETs in 2024 with breakdown voltages up to 2200 V and power figures of merit exceeding 150 MW/cm^2 [32]. These devices show power density superior to both SiC and GaN alternatives.

However, β-Ga_2O_3 faces two fundamental challenges. First, its relatively low thermal conductivity (0.1–0.3 W/cm·K) is approximately 10–30$\times$ lower than SiC, necessitating sophisticated thermal management solutions including heterogeneous integration with high-thermal-conductivity substrates. Second, the absence of effective p-type doping limits device architectures to unipolar configurations such as Schottky Barrier Diodes (SBDs) and Field-Effect Transistors (FETs). Recent research has explored heterostructures with NiO_x and other p-type materials to enable bipolar operation [33].

The global market for high-purity β-Ga_2O_3 power devices is projected to grow at a Compound Annual Growth Rate (CAGR) of approximately 24.5% from 2024 to 2033, with applications initially targeting the 600 V–3.3 kV range for EV power systems, solar inverters, and grid interface equipment.

3.2. Aluminum Nitride (AlN)

Aluminum nitride possesses the highest critical electric field (15 MV/cm) among practical UWBG semiconductors, enabling exceptionally thin drift regions and low on-resistance for a given breakdown voltage [34]. Its bandgap of 6.2 eV and Johnson's Figure of Merit 5$\times$ higher than GaN make it particularly attractive for both high-power switching and high-frequency applications.

A major breakthrough was reported at the IEEE International Electron Devices Meeting (IEDM) in December 2023, where researchers from Nagoya University demonstrated AlN-based diodes capable of withstanding electric fields of 7.3 MV/cm—approximately twice the capability of SiC or GaN [19]. This achievement utilized the Distributed Polarization Doping (DPD) technique, which enables effective n-type and p-type doping in AlGaN alloys without conventional impurity dopants, circumventing AlN's historically problematic doping challenges.

In 2024, a German research consortium led by Fraunhofer IISB successfully demonstrated a complete value chain for AlN-based devices in Europe [35]. The consortium grew AlN crystals up to 43 mm diameter, processed them into polished wafers, and fabricated AlN/GaN high-electron-mobility transistors (HEMTs) with breakdown voltages up to 2200 V and power densities superior to both SiC and GaN devices. These AlN/GaN HEMTs offer up to 3000$\times$ lower conduction losses than silicon and are approximately 10$\times$ more efficient than SiC transistors.

Crystal IS has achieved production of 100 mm (4-inch) diameter single-crystal AlN substrates with 99% usable area, a significant milestone toward commercial viability [36]. Researchers at Nagoya University project commercialization of AlN-based power devices in the 2030s, contingent on resolving remaining challenges in ohmic contact formation and scaling manufacturing processes.

3.3. Diamond

Diamond represents the ultimate semiconductor material, offering an unparalleled combination of an ultra-wide bandgap (5.5 eV), the highest thermal conductivity of any material (22–23 W/cm·K),

© 2025 by the author(s). Distributed under a Creative Commons CC BY license.

Preprints.org (www.preprints.org) | NOT PEER-REVIEWED | Posted: 29 January 2026 doi:10.20944/preprints202601.2280.v1

exceptional carrier mobility (4500 cm^2/Vs for electrons, 3800 cm^2/Vs for holes), and a theoretical critical electric field of 10–20 MV/cm [37]. These properties yield a BFOM 50,000× that of silicon, positioning diamond as the long-term solution for extreme power density applications.

Significant progress has been made in diamond device development. Researchers at the University of Illinois Urbana-Champaign demonstrated diamond Schottky barrier diodes with the highest reported breakdown voltage (4.6 kV at 0.01 mA/mm) and lowest leakage current among diamond devices [20]. Japan's National Institute for Materials Science (NIMS) achieved another milestone in 2024 with the world's first n-channel diamond MOSFET, exhibiting field-effect mobility over 150 cm^2/Vs at 573 K—the highest among all n-channel MOSFETs based on wide-bandgap semiconductors [21].

Japanese institutions are leading diamond semiconductor commercialization efforts. Saga University developed the world's first diamond-based power device in 2023 in collaboration with the Japan Aerospace Exploration Agency (JAXA) for high-frequency space communication applications. Orbray has developed mass-production technology for 2-inch diamond wafers and is progressing toward 4-inch substrates, with partnerships including Toyota and Denso supporting onboard power device development expected in the 2030s [38].

Diamond's primary challenges include the difficulty of n-type doping due to high activation energies, the lack of a mature manufacturing ecosystem, and substrate availability limitations. However, advances in chemical vapor deposition (CVD) growth and recent n-channel MOSFET demonstrations suggest these barriers are being systematically addressed.

3.4. Cubic Boron Nitride (c-BN)

Cubic boron nitride represents a compelling UWBG semiconductor that combines many of diamond's exceptional properties with potentially superior doping characteristics [39,40]. With a bandgap of 6.4 eV—the highest among practical semiconductors—and a theoretical critical electric field of 12 MV/cm, c-BN offers extraordinary high-voltage capability. Its thermal conductivity of 13 W/cm·K, while lower than diamond, significantly exceeds that of SiC and GaN.

The key advantage of c-BN over diamond lies in its doping flexibility. Both n-type and p-type doping have been demonstrated with activation energies lower than those in diamond, potentially enabling efficient bipolar devices [41]. Silicon substituting on the boron site (Si_B) serves as an effective n-type dopant, while beryllium and magnesium provide p-type conductivity. Recent work at North Carolina State University demonstrated n-type conductivity with carbon doping concentrations ranging from 2×10^{19} to 7×10^{21} cm^{-3}, achieving semiconductor-like resistivity profiles [42].

Manufacturing c-BN remains challenging. Conventional High-Pressure, High-Temperature (HPHT) synthesis at >1,150°C and >2.5 GPa produces only millimeter-scale crystals—far below the centimeter-scale wafers required for electronics manufacturing [43]. However, breakthrough fabrication techniques are emerging:

Pulsed Laser Annealing (PLA): Researchers have demonstrated direct conversion of hexagonal BN (h-BN) into phase-pure single-crystal c-BN using nanosecond laser pulses, achieving conversion in approximately 200 ns at ambient pressure [44]. This technique can produce epitaxial c-BN thin films on sapphire substrates with controlled doping.

Solution growth: Texas Tech University, with Department of Energy (DOE) funding, is developing autoclave-based solution growth methods that could enable scalable production of electronic-grade c-BN wafers for extreme-temperature electronics [45].

Diamond/c-BN heterostructures: First-principles calculations indicate that diamond/c-BN heterojunctions can form high-density two-dimensional carrier gases at the interface, potentially enabling high-frequency, high-power devices that leverage both materials' advantages [46].

The projected applications for c-BN power devices include ultra-high-voltage (>10 kV) grid infrastructure, extreme-environment electronics for aerospace and geothermal applications, and next-generation smart grid transformers. While commercialization remains in the ≥2035 timeframe, c-BN's combination of UWBG properties and doping flexibility positions it as a potential ultimate solution for extreme power electronics.

© 2025 by the author(s). Distributed under a Creative Commons CC BY license.

Table 5 summarizes the development status and projected commercialization timeline for UWBG materials.

Table 5. UWBG Materials Development Status and Commercialization Timeline.

Parameter	β-Ga_2O_3	AlN	c-BN	Diamond
Wafer Size (Comm.)	4-inch	4-inch	<1 mm	2-inch
Best Device V_{BR}	2.3 kV	2.2 kV	N/A	4.6 kV
TRL Level	4–5	3–4	2–3	3–4
E_g (eV)	4.9	6.2	6.4	5.5
κ (W/cm·K)	0.1–0.3	2.85	13	22–23
Primary Challenge	Low κ	Doping/Contacts	Substrate size	n-type doping
Target Applications	600V–3.3kV	10kV+, RF	>10kV, extreme	Extreme power
Projected Commerc.	2027–2030	2030s	≥2035	2030–2035

4. WBG Device Architectures: SiC and GaN

The commercial landscape of WBG semiconductors has matured significantly [47,48]. This section presents device configurations for both SiC and GaN technologies.

4.1. SiC Device Configurations

Silicon Carbide power devices have evolved into several mature device architectures, each offering distinct advantages for specific application requirements [5,17]. Figure 6 presents the classification of commercial SiC power devices.

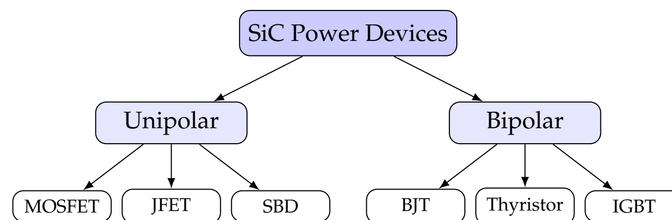

Figure 6. Classification of SiC power devices

4.1.1. SiC MOSFET Structure

The SiC MOSFET is the dominant commercial device, offering normally-off operation with voltage-controlled switching [49]. The planar MOSFET suffers from the "JFET effect"—the narrow conduction path between adjacent p-wells increases on-resistance. Trench MOSFETs eliminate this limitation by orienting the channel vertically, achieving 30–50% lower specific on-resistance [50]. The on-resistance of a SiC MOSFET can be expressed as:

$$R_{DS(on)} = R_{ch} + R_{JFET} + R_{drift} + R_{sub} + R_{contact} \tag{7}$$

where R_{ch} is channel resistance, R_{JFET} is the JFET region resistance (eliminated in trench designs), R_{drift} is drift region resistance, R_{sub} is substrate resistance, and $R_{contact}$ represents contact resistances. Figure 7 illustrates the planar and trench SiC MOSFET structures.

© 2025 by the author(s). Distributed under a Creative Commons CC BY license.

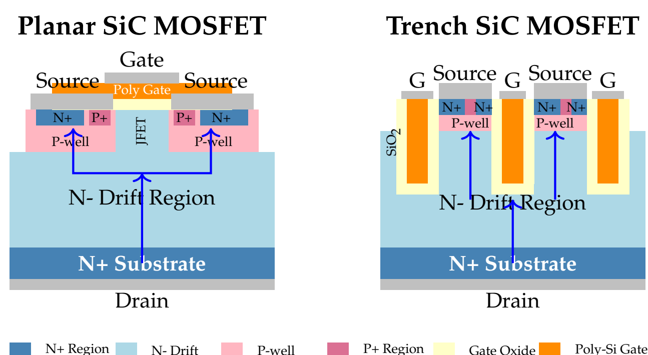

Figure 7. Planar SiC MOSFET and Trench SiC MOSFET Structures

4.2. GaN Device Configurations

Figure 8 presents the classification of GaN HEMT devices.

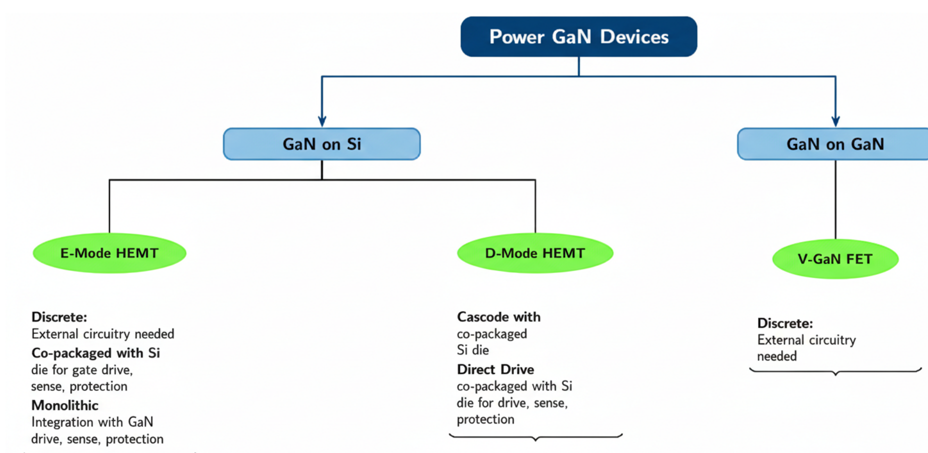

Figure 8. Classification of GaN HEMTs devices.

Figure 9 illustrates the different types of GaN devices including normally-on and normally-off configurations.

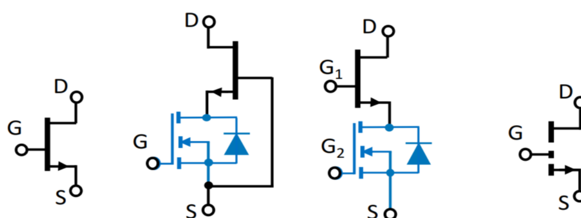

Figure 9. Different types of GaN devices: Normally-on (d-mode), Normally-off Cascode (d-mode), Direct Drive (d-mode), Normally off (e-mode)

4.2.1. Depletion-Mode (D-Mode) GaN HEMTs

D-mode devices are inherently normally-on, requiring a negative gate voltage to turn off. The Two-Dimensional Electron Gas (2DEG) at the AlGaN/GaN interface provides exceptionally high electron mobility and carrier density. Figure 10 shows the internal structure of a D-mode GaN HEMT, as described in detail in [51].

© 2025 by the author(s). Distributed under a Creative Commons CC BY license.

Preprints.org (www.preprints.org) | NOT PEER-REVIEWED | Posted: 29 January 2026
doi:10.20944/preprints202601.2280.v1

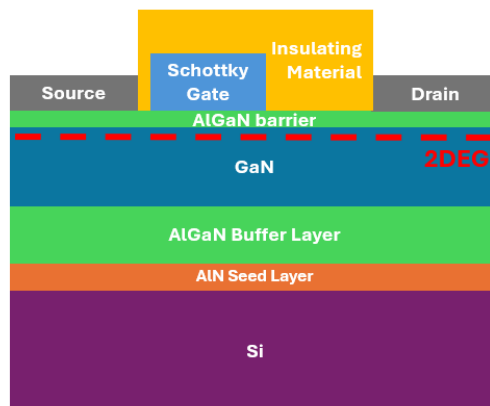

Figure 10. GaN D-Mode Internal Structure

4.2.2. Enhancement-Mode (E-Mode) GaN HEMTs

E-mode devices achieve normally-off operation through p-doped GaN gate structures [52,53]. This configuration is preferred for power electronics applications due to inherent safety during start-up and fault conditions. Figure 11 shows the internal structure as described in detail in [51].

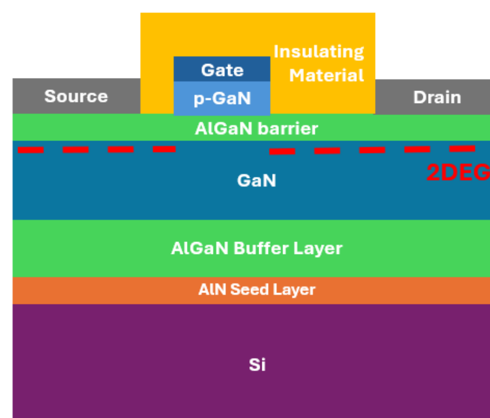

Figure 11. GaN E-Mode Internal Structure

4.2.3. Vertical GaN Power Devices

While lateral GaN HEMTs dominate the commercial market for voltages up to 650 V, vertical GaN devices are emerging as critical enablers for medium-voltage applications (1.2–10 kV) where they compete directly with SiC [54]. Unlike lateral devices where voltage scaling requires proportionally larger chip area, vertical GaN conducts current perpendicular to the substrate surface, allowing breakdown voltage to increase through drift layer thickness while maintaining compact chip dimensions.

Recent advances have demonstrated impressive performance milestones. Onsemi unveiled vertical GaN (vGaN) technology in December 2024, featuring 1,200 V-class devices capable of reducing system losses by nearly 50% compared to lateral GaN, while achieving approximately 3× smaller die size [55]. Toyoda Gosei demonstrated vertical GaN transistors with operating currents exceeding 50 A—the highest reported for vertical GaN—enabling MHz-frequency operation in compact packages [56].

Vertical GaN architectures include trench MOSFETs (T-MOSFETs), Current Aperture Vertical Electron Transistors (CAVETs), and vertical Junction Field-Effect Transistors (JFETs). The 1.2 kV vertical GaN fin-channel JFET has emerged as a particularly promising device, offering normally-off operation, avalanche capability, and no dynamic R_{on} degradation—addressing one of the primary reliability concerns of lateral GaN HEMTs [57].

© 2025 by the author(s). Distributed under a Creative Commons CC BY license.

Preprints.org (www.preprints.org) | NOT PEER-REVIEWED | Posted: 29 January 2026 doi:10.20944/preprints202601.2280.v1

Key challenges for vertical GaN include the limited availability of native GaN substrates (currently 2–4 inch), high substrate costs, and the difficulty of achieving low background doping ($< 1.5 \times 10^{16}$ cm^{-3}) in thick drift layers required for 1.2 kV+ operation. However, advances in GaN-on-engineered-substrate technology are enabling 200 mm CMOS-compatible fabrication pathways that could dramatically reduce costs [58].

4.2.4. GaN Bidirectional Switches (BDS)

Monolithic bidirectional switches represent a paradigm shift in power semiconductor technology, enabling four-quadrant operation—bidirectional current flow and bipolar voltage blocking—from a single device [59]. While conventional approaches require four discrete transistors in back-to-back configurations (doubling $R_{DS(on)}$ and component count), GaN BDS devices leverage the lateral HEMT structure to integrate two opposing gates sharing a common drift region. An example is provided in the following Section 5.1.2.

Infineon's CoolGaN BDS family, announced in 2024, offers devices at 40 V, 650 V, and 850 V ratings with four operational modes: full conduction, full blocking, and two diode modes (forward and reverse blocking) [60]. Navitas announced production-released 650 V bidirectional GaNFast ICs in March 2025, targeting single-stage power conversion topologies [61].

Key applications for GaN BDS include matrix converters (direct AC-AC conversion without DC-link), Vienna rectifiers (three-level PFC with bidirectional current capability), T-type inverters (three-level topologies for solar and motor drive applications), Current-Source Inverters (CSI) for high-power motor drives and High-Voltage Direct Current (HVDC) transmission, and Highly Efficient and Reliable Inverter Concept (HERIC) inverters for Photovoltaic (PV) applications with reactive power capability.

Table 6 summarizes the key differences between WBG device technologies.

Table 6. Comparison of WBG and Si Device Characteristics, data taken from [4,47].

Parameter	GaN HEMT	GaN Cas.	SiC MOS	Si IGBT
Voltage (V)	600–650	600–900	650–3300	600–6500
Current (A)	1–90	10–60	5–200	10–3600
$R_{on} \cdot A$ (mΩcm^2)	1–5	3–8	3–15	—
Max f_{sw} (MHz)	1–40	0.5–10	0.1–2	0.02–0.1
dv/dt (V/ns)	50–200	30–100	20–100	1–20
Q_g (nC)	1–20	10–50	20–300	100–5000
Max T_j (°C)	150–175	150	175–200	175
Rev. Recovery	None	Limited	Moderate	V. High
FOM ($R \cdot Q$)	Best	Good	Good	Poor
Cost ($/A)	Medium	Med-High	High	Low

5. Converter Topologies for WBG Devices

5.1. SiC Converter Topologies

SiC devices excel in high-power, high-voltage converter applications where their superior breakdown voltage and thermal conductivity provide significant advantages over both Si and GaN alternatives [62].

5.1.1. Three-Phase Traction Inverter

The three-phase voltage source inverter is the dominant topology for electric vehicle traction drives [63]. Figure 12 shows a SiC-based traction inverter configuration.

© 2025 by the author(s). Distributed under a Creative Commons CC BY license.

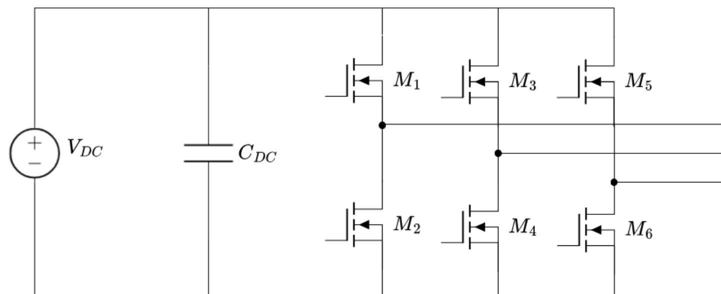

Figure 12. SiC-based three-phase traction inverter for electric vehicle applications, adapted from [64].

The power loss in each SiC MOSFET comprises conduction and switching components:

$$P_{loss} = I_{rms}^2 \cdot R_{DS(on)}(T_j) + f_{sw}(E_{on} + E_{off}) \tag{8}$$

SiC enables switching frequencies of 10–20 kHz in traction applications (versus 5–10 kHz for Si IGBTs), reducing motor current ripple and acoustic noise while maintaining >98% inverter efficiency [11].

5.1.2. DC Fast Charging Converter

DC fast charging stations (50–350 kW) leverage SiC's high-voltage capability and efficiency [65]. Figure 13 shows a typical three-phase Vienna rectifier front-end with isolated DC-DC stage.

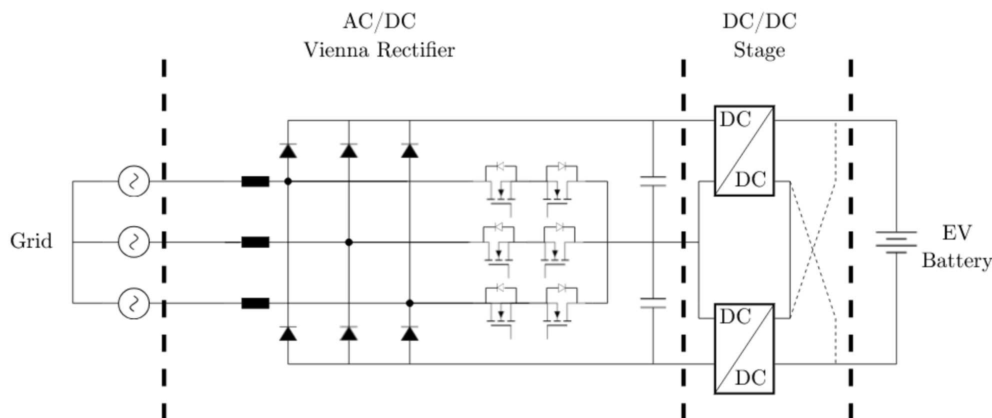

Figure 13. SiC-based DC fast charging architecture: Vienna rectifier PFC front-end with isolated DC-DC converter, adapted from [66].

The Vienna rectifier achieves near-unity power factor with reduced switch count compared to conventional Pulse Width Modulation (PWM) rectifiers, while SiC enables operation at 30–50 kHz for compact magnetic design.

5.1.3. Grid-Tied Solar Inverter

Central and string inverters for photovoltaic applications benefit from SiC's efficiency at partial load conditions [67]. Figure 14 shows a three-level T-type inverter topology.

© 2025 by the author(s). Distributed under a Creative Commons CC BY license.

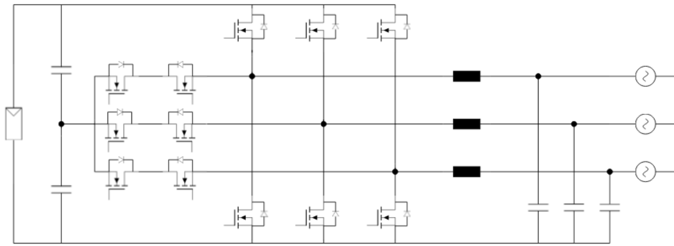

Figure 14. SiC-based T-type three-level inverter for grid-tied PV applications, adapted from [68]

Three-level topologies reduce the voltage stress on each device to $V_{DC}/2$, enabling higher DC-link voltages (up to 1500 V for utility-scale installations) while maintaining acceptable dv/dt levels. The output voltage Total Harmonic Distortion (THD) is significantly improved:

$$THD_{3L} \approx \frac{THD_{2L}}{2} \tag{9}$$

5.2. GaN Converter Topologies

Implementing GaN devices in power converter topologies requires careful consideration of their unique characteristics [69,70]. Printed Circuit Board (PCB) layout is critical for achieving optimal performance.

5.2.1. Buck Converters

The synchronous buck converter represents an ideal topology for demonstrating GaN advantages [71]. The inductance value is selected to maintain Continuous Conduction Mode (CCM) operation [72]:

$$L = \frac{V_{out}(V_{in} - V_{out})}{V_{in} \cdot f_{sw} \cdot \Delta I_L} \tag{10}$$

Output voltage ripple is given by:

$$\Delta V_{out} = \Delta I_L \cdot \text{ESR} + \frac{\Delta I_L}{8 f_{sw} C_{out}} \tag{11}$$

5.2.2. Interleaved Buck Converters

Interleaving multiple phases provides significant advantages in high-current applications [73]. The current imbalance between phases is [74]:

$$\Delta I_{imbalance} = I_{out} \cdot \frac{\Delta L/L + \Delta R_{DS(on)}/R_{DS(on)}}{N} \tag{12}$$

5.2.3. Dual Active Bridge Converters

The DAB converter has emerged as a leading topology for bidirectional isolated DC-DC conversion [75,76]. Zero Voltage Switching (ZVS) operation is achievable over a wide load range. The average power transfer is [77]:

$$P = \frac{nV_1V_2}{2\pi f_s L_s}\phi\left(1 - \frac{|\phi|}{\pi}\right) \tag{13}$$

The inductor current evolution is:

$$i_{Ls}(t) = i_{Ls}(0) + \frac{1}{L_s}\int_0^t v_{Ls}(\tau)d\tau \tag{14}$$

© 2025 by the author(s). Distributed under a Creative Commons CC BY license.

5.2.4. Multilevel DAB Topologies

For medium-voltage applications (>1 kV), multilevel DAB topologies extend capabilities [78]. The three-level Neutral Point Clamped (NPC) DAB reduces voltage stress on individual switches:

$$V_{switch,3L} = \frac{V_{dc}}{2} < V_{switch,2L} = V_{dc} \tag{15}$$

5.3. GaN Technology Evolution: Vertical GaN and BDS for Converter Topologies

While the preceding sections focused on established SiC and lateral GaN technologies, this section examines how emerging GaN device architectures—specifically vertical GaN and monolithic bidirectional switches (BDS)—are reshaping converter design possibilities. Table 7 provides a topology-by-topology analysis of how these emerging technologies compare to established SiC solutions.

5.3.1. Vertical GaN: Challenging SiC in Medium-Voltage Applications

Vertical GaN power devices represent a paradigm shift from traditional lateral GaN-on-Si HEMTs, enabling operation at 1.2 kV and beyond—voltage classes currently dominated by SiC [54,55]. Unlike lateral devices where breakdown voltage scales with chip area, vertical GaN conducts current perpendicular to the substrate, allowing voltage scaling through drift layer thickness while maintaining compact die dimensions.

Topology Implications:

Three-Phase Traction Inverters: The traditional domain of SiC MOSFETs, traction inverters are a prime target for vertical GaN. Onsemi's 1,200 V vGaN technology demonstrates nearly 50% lower losses compared to lateral GaN and approximately 3× smaller die size [55]. The superior switching figure of merit ($R_{on} \times Q_g$) enables switching frequencies of 50–100 kHz while maintaining efficiency above 99%, compared to 10–20 kHz typical for SiC traction inverters. The reduced Q_{oss} also simplifies soft-switching in resonant topologies.

DC Fast Charging (Vienna Rectifier and DAB): For 800 V battery systems, 1.2 kV vertical GaN enables single-device implementations without series stacking. The absence of dynamic R_{on} degradation—a key reliability concern in lateral GaN HEMTs [79]—makes vertical GaN particularly attractive for high duty-cycle applications like DC fast chargers.

Grid-Tied Inverters: Medium-voltage applications (1500 V DC-link for utility-scale PV) require 3.3 kV device ratings. Vertical GaN development is progressing toward this voltage class, with 2.3 kV demonstrations reported in research [58]. When commercially available, vertical GaN could challenge SiC in this application through superior switching speed.

Key Advantages over Lateral GaN:

- Voltage scaling through drift layer thickness rather than lateral area
- No dynamic R_{on} degradation (no surface traps)
- Avalanche capability similar to SiC MOSFETs
- Reduced chip area for given voltage/current rating

Current Limitations:

- Limited substrate availability (2–4 inch GaN-on-GaN)
- Higher substrate cost compared to SiC or GaN-on-Si
- Manufacturing maturity gap (TRL 4–5 vs. TRL 8–9 for SiC)
- Projected commercialization: 2026–2028 for 1.2 kV class

5.3.2. Bidirectional GaN Switches: Enabling Single-Stage Power Conversion

Monolithic bidirectional switches (BDS) represent perhaps the most transformative GaN innovation for power converter topologies [59,61]. By integrating four-quadrant operation (bidirectional current flow and bipolar voltage blocking) into a single device, GaN BDS enables entirely new converter architectures previously impractical with discrete devices.

© 2025 by the author(s). Distributed under a Creative Commons CC BY license.

Preprints.org (www.preprints.org) | NOT PEER-REVIEWED | Posted: 29 January 2026 doi:10.20944/preprints202601.2280.v1

Revolutionary Topology Enablement:

Single-Stage AC-DC Conversion: Traditional two-stage converters (PFC + isolated DC-DC) require intermediate DC-link capacitors—often the largest, heaviest, and least reliable components. GaN BDS enables single-stage isolated conversion through cycloconverter and matrix-type topologies, eliminating the DC-link entirely [60]. Benefits include:

- 40–50% size reduction in EV on-board chargers
- Elimination of electrolytic capacitors (improved reliability)
- Inherent bidirectional power flow (V2G capability)
- Higher efficiency through single-stage conversion

Matrix Converters (Direct AC-AC): Matrix converters provide direct frequency conversion without DC-link, but historically required complex discrete switch arrays. Each bidirectional switch position previously needed four discrete transistors in anti-series/anti-parallel configuration, quadrupling component count and on-resistance. A single GaN BDS replaces this four-device array, making matrix converters practical for:

- Variable-frequency motor drives
- Solid-state transformers
- Grid frequency conversion

Vienna Rectifiers and T-Type Inverters: These three-level topologies require bidirectional switches for the neutral-point connection. Replacing back-to-back discrete switches with GaN BDS provides:

- 50% reduction in on-resistance for bidirectional current path
- Simplified gate drive (two isolated channels vs. four)
- Higher switching frequency capability (>100 kHz vs. 30–50 kHz)
- Reduced PCB complexity and parasitic inductance

HERIC Inverters for PV: The HERIC topology uses bidirectional switches to decouple the PV array from the grid during freewheeling periods, reducing common-mode leakage current. GaN BDS enables MHz-frequency operation of HERIC inverters while supporting reactive power compensation for grid support functions.

Current-Source Inverters (CSI): CSI topologies require bidirectional voltage blocking, traditionally achieved with series diodes that increase losses. GaN BDS provides native bidirectional blocking with lower on-resistance, enabling CSI adoption for high-power motor drives with improved efficiency and inherent short-circuit protection [80].

Table 7. GaN Technology Evolution: Impact on Converter Topologies vs. Established SiC.

Topology	Current SiC Solution	Vertical GaN Potential	GaN BDS Potential	Timeline
Traction Inverter	1.2 kV SiC MOSFET, 10–20 kHz	1.2 kV vGaN, 50–100 kHz, 50% lower losses	Not applicable	vGaN: 2027–2029
Vienna Rectifier	Back-to-back SiC, 30–50 kHz	Higher frequency, smaller magnetics	Single-device solution, 100 kHz+	BDS: 2025–2026
DAB Converter	SiC for >50 kW, ZVS operation	Smaller transformer, higher frequency	Single-stage capability	vGaN: 2028+
T-Type Inverter	Discrete SiC neutral switches	Enhanced switching speed	50% lower R_{on}, simplified drive	BDS: Available now
Matrix Converter	Complex discrete arrays	N/A	Revolutionary: single-device BDS	BDS: 2025–2026
HERIC (PV)	Discrete Si/SiC switches	N/A	MHz operation, grid support	BDS: Available now
CSI Motor Drive	SiC + series diodes	Native blocking, lower losses	Native bidirectional blocking	Both: 2027+
Single-Stage OBC	Two-stage (PFC + DC-DC)	N/A	Eliminates DC-link capacitor	BDS: 2025–2026

© 2025 by the author(s). Distributed under a Creative Commons CC BY license.

Preprints.org (www.preprints.org) | NOT PEER-REVIEWED | Posted: 29 January 2026 doi:10.20944/preprints202601.2280.v1

5.3.3. Design Guidelines for Technology Selection

Based on the analysis of current SiC capabilities and emerging GaN technologies, the following guidelines assist designers in technology selection:

Continue with SiC when:

- Voltage requirements exceed 1.2 kV (until vertical GaN matures)
- High current (>100 A) with established supply chain is required
- Short-circuit withstand capability is critical
- Junction temperatures exceeding 175°C are needed
- Proven reliability and qualification data are mandatory

Consider Vertical GaN when (2027+ timeframe):

- Maximum switching frequency above 50 kHz is beneficial
- Power density is the primary optimization target
- Dynamic R_{on} stability is critical (continuous hard-switching)
- Avalanche capability with superior switching FOM is desired
- Voltage class is 650 V–1.2 kV

Adopt GaN BDS when:

- Bidirectional current flow and voltage blocking are required
- Single-stage conversion topology is feasible
- DC-link capacitor elimination is valuable (size, reliability, cost)
- Vienna, T-type, HERIC, or matrix topologies are employed
- Switching frequency above 100 kHz is targeted
- Grid-connected applications require reactive power support

5.3.4. Market and Technology Outlook

The convergence of vertical GaN and BDS technologies is expected to accelerate the displacement of SiC in specific application segments while opening entirely new topology possibilities. Key milestones include:

- **2025:** Commercial 650 V GaN BDS devices (Infineon, Navitas); initial vertical GaN sampling at 700–1200 V
- **2026–2027:** Production vertical GaN for EV traction; BDS adoption in solar microinverters
- **2028–2030:** Vertical GaN challenging SiC in medium-voltage segments; matrix converters becoming mainstream
- **2030+:** Potential vertical GaN extension to 3.3 kV for grid applications

The combination of vertical GaN for high-voltage unidirectional applications and BDS for bidirectional topologies positions GaN technology as a comprehensive competitor to SiC across the medium-voltage power electronics landscape, rather than remaining confined to the sub-650 V market segment.

6. SiC vs. GaN: Comprehensive Comparison

6.1. Topology-Specific Comparison

The selection between SiC and GaN devices depends critically on the converter topology, power level, voltage class, and switching frequency requirements. Table 8 provides a comprehensive comparison for the major power converter topologies.

© 2025 by the author(s). Distributed under a Creative Commons CC BY license.

Preprints.org (www.preprints.org) | NOT PEER-REVIEWED | Posted: 29 January 2026 doi:10.20944/preprints202601.2280.v1

Table 8. SiC vs. GaN Comparison for Major Power Converter Topologies.

Topology	SiC Advantages	GaN Advantages	Recommended
Two-Level VSI	Higher voltage (1.2–3.3 kV), better thermal	Lower switching losses, smaller passives	SiC (>100 kW)
Buck (<1 kW)	Better thermal margin	10× lower Q_g, MHz operation	GaN
Buck (>10 kW)	Higher current handling	Lower switching losses at 100–500 kHz	SiC
Interleaved	Better current sharing, thermal stability	Phase current cancellation, smaller magnetics	Application dependent
DAB (<20 kW)	Wide ZVS range	>500 kHz, smaller transformer	GaN
DAB (>50 kW)	1.2 kV/>100 A devices	Lower turn-off losses	SiC
Vienna Rectifier	Higher voltage margin	Lower THD with higher f_{sw}	GaN (<30 kW); SiC (>30 kW)
T-Type/NPC	1700 V devices for 1500 V PV	BDS enables single-package solution	GaN (resid.); SiC (utility)
LLC Resonant	Wide input range, stable C_{oss}	Very low C_{oss}, enables >1 MHz	GaN

6.2. Efficiency and Loss Comparison

The total losses in a power converter include conduction and switching components. For a given topology, the device selection significantly impacts both:

Conduction losses: SiC MOSFETs exhibit positive temperature coefficient of $R_{DS(on)}$, improving current sharing in parallel configurations but increasing losses at elevated temperatures. GaN HEMTs have flatter temperature dependence and lower specific on-resistance ($R_{on} \cdot A$) below 650 V, but require more devices in parallel for high-current applications.

Switching losses: GaN devices achieve 3–10× lower switching energy (E_{sw}) than equivalently-rated SiC MOSFETs due to smaller gate charge and output capacitance. This advantage enables proportionally higher switching frequencies, reducing passive component size according to:

$$L_{min} \propto \frac{1}{f_{sw}}, \quad C_{min} \propto \frac{1}{f_{sw}} \tag{16}$$

6.3. Application-Specific Recommendations

Based on the comprehensive analysis, the following guidelines emerge:

EV Traction Inverter (>100 kW, 400–800 V): SiC MOSFET is the clear choice due to 1.2 kV voltage rating, superior thermal management, and proven reliability. GaN may enter this space with vertical GaN devices in the 2027–2030 timeframe.

On-Board Charger (3.3–22 kW): GaN preferred for 6.6–11 kW class where MHz switching enables significant size reduction. SiC competitive at 22 kW and above where thermal management dominates.

DC Fast Charging (>50 kW): SiC dominates due to 800–1000 V DC-link requirements and high power levels.

Server/Telecom PSU (1–3 kW): GaN preferred for highest power density and efficiency in space-constrained applications.

Solar String Inverter (5–20 kW): GaN increasingly competitive with SiC, offering efficiency >99% with smaller EMI filters. BDS-enabled single-stage topologies emerging.

Motor Drives (<10 kW): GaN enables higher PWM frequencies reducing motor losses and acoustic noise. Current-source inverters with GaN BDS offer EMI advantages.

© 2025 by the author(s). Distributed under a Creative Commons CC BY license.

Preprints.org (www.preprints.org) | NOT PEER-REVIEWED | Posted: 29 January 2026 doi:10.20944/preprints202601.2280.v1

6.4. Gate Driver Requirements

The fundamental differences between Si, SiC, and GaN devices necessitate distinct gate driver designs. The key factor differentiating WBG and Si driving characteristics is the much faster transient capability of WBG devices, requiring shorter driver rise/fall times and propagation delays [81]. Table 9 provides a comprehensive comparison of gate driver requirements.

Table 9. Gate Driver Requirements Comparison: Si vs. SiC vs. GaN, data taken from [81–83].

Parameter	Si MOSFET/IGBT	SiC MOSFET	GaN HEMT
V_{GS} Turn-on	+10 to +15 V	+15 to +20 V	+5 to +6 V
V_{GS} Turn-off	0 V	−3 to −5 V	0 V
Gate Charge (Q_g)	50–500 nC	20–100 nC	1–10 nC
Peak Drive Current	1–4 A	4–10 A	1–5 A
Propagation Delay	50–200 ns	20–50 ns	<20 ns
dV/dt Immunity	10–50 V/ns	50–150 V/ns	100–300 V/ns
Negative Bias Req.	Optional	Required	Not Required
Miller Plateau	Flat, defined	Higher, not flat	Low, fast
V_{th} Range	2–4 V	1.5–4 V	1–2 V

6.4.1. SiC MOSFET Gate Drive Considerations

SiC MOSFETs require careful gate drive optimization to achieve reliable high-speed switching [82]. The recommended gate-source voltage is typically +18 to +20 V for turn-on to minimize on-resistance, with −3 to −5 V for turn-off to ensure complete channel depletion and prevent spurious turn-on from dV/dt-induced Miller current. The non-flat Miller plateau characteristic of SiC MOSFETs, occurring at higher V_{GS} than silicon devices, is a consequence of the lower transconductance inherent to SiC. SiC devices also exhibit higher internal gate resistance ($R_{G,int}$), which can limit switching speed if the external gate driver impedance is not sufficiently low.

Key protection features for SiC gate drivers include desaturation detection with response times below 200 ns for short-circuit protection, active Miller clamping to prevent false turn-on during high dV/dt transients, and Under-Voltage Lockout (UVLO) for both positive and negative supply rails.

6.4.2. GaN HEMT Gate Drive Considerations

Enhancement-mode GaN HEMTs present unique gate drive challenges due to their low threshold voltage (typically 1–2 V), limited gate voltage range (maximum V_{GS} of 6–7 V), and extremely fast switching capability [18,81]. The gate structure in p-GaN HEMTs is essentially a forward-biased diode, which can conduct significant gate current if V_{GS} exceeds the forward voltage.

GaN devices benefit significantly from integrated gate drivers that minimize parasitic inductance in the gate loop. Products such as Navitas GaNSafe and EPC eGaN ICs integrate the gate driver with the power transistor in a single package, achieving zero gate-source loop inductance and enabling switching frequencies up to 2 MHz [84]. For discrete GaN implementations, the gate driver should be placed as close as possible to the device with minimal loop area, and Common-Mode Transient Immunity (CMTI) exceeding 100 V/ns is essential.

7. System-Level Implications and Benefits

The adoption of WBG devices yields measurable improvements that extend well beyond simple device-level metrics [8,85].

7.1. Efficiency Improvements and Economic Impact

WBG devices enable efficiency gains of 2–5% in most power conversion applications. Table 10 quantifies the economic advantages across different application sectors.

© 2025 by the author(s). Distributed under a Creative Commons CC BY license.

Table 10. Economic Benefits of WBG Adoption Across Application Sectors.

Sector	Application	η Impr.	Savings	Payback
Data Center	Server PSU (10 MW)	94→97%	$450k/yr	1.5 yr
EV	Traction inverter	96→99%	+20 km	Immed.
Solar PV	String inv. (1 MW)	96→98.5%	$35k/yr	2 yr
Industrial	Variable Frequency Drive (VFD) (500 kW)	95→98%	$22k/yr	2.5 yr
Telecom	5G base station	92→95%	$8k/site	1.8 yr
Aerospace	Aux. power unit	93→97%	−15 kg	Immed.

7.2. Passive Component Reduction

Operating at higher switching frequencies enables proportional reduction in magnetic component size [86,87]:

$$V_{mag} \propto \frac{P \cdot \Delta B}{f_{sw}} \tag{17}$$

Increasing switching frequency from 20–50 kHz to 200–500 kHz (SiC) or MHz ranges (GaN) enables 5–20× reduction in magnetic component volume [88].

7.3. Key Performance Indicators Comparison

Table 11 provides a comprehensive comparison of Key Performance Indicators (KPIs) between silicon and WBG systems [8].

Table 11. Key Performance Indicators: Silicon vs. WBG Comparison, data taken from [8].

KPI	Silicon	WBG
Peak efficiency (η_{peak})	94–97%	98–99.5%
Power density	3–8 kW/L	15–50 kW/L
Specific power	2–5 kW/kg	8–20 kW/kg
Switching frequency (f_{sw})	20–100 kHz	0.2–2 MHz
Maximum junction temp. ($T_{j,max}$)	150°C	175–200°C
Total harmonic distortion (THD)	3–8%	1–3%
Voltage slew rate (dv/dt)	5–15 kV/μs	50–200 kV/μs
Current slew rate (di/dt)	1–5 kA/μs	10–50 kA/μs

7.4. SiC System Benefits

The adoption of SiC technology delivers quantifiable advantages with respect to Silicon devices across multiple system dimensions [8]:

Efficiency improvements: SiC MOSFETs achieve 2–5% higher conversion efficiency compared to Si IGBTs in high-power applications, primarily due to elimination of tail current losses and reduced conduction losses at elevated temperatures. In EV traction inverters, this translates to 5–8% extended driving range [11].

Power density: The combination of reduced losses and higher junction temperature capability ($T_{j,max}$ = 175–200°C vs. 150°C for Si) enables 30–50% reduction in heatsink volume. Wolfspeed's XM3 power module achieves 3× the power density of equivalent Si IGBT modules [89].

Thermal management simplification: Higher-temperature operation reduces the temperature differential between junction and ambient, enabling passive cooling solutions in applications previously requiring active cooling. This eliminates fan maintenance, acoustic noise, and reliability concerns associated with moving parts.

© 2025 by the author(s). Distributed under a Creative Commons CC BY license.

System cost reduction: While SiC devices carry a 2–3× premium over Si equivalents, total system cost is often reduced by 10–25% when considering smaller passive components (inductors, capacitors, heatsinks), simplified cooling systems, and reduced enclosure size [8].

8. Application Landscape and Case Studies

The distinct characteristics of SiC and GaN have led to natural market segmentation based on voltage class, power level, and switching frequency requirements [47,90].

8.1. Automotive and Transportation Applications

SiC transistors are widely implemented in traction inverters for hybrid and electric vehicles—Tesla, for instance, has utilized SiC technology since 2017, achieving 5-8% improvement in vehicle range through increased inverter efficiency [11,12]. The transition from Si IGBTs to SiC MOSFETs in automotive applications has been driven by multiple factors: reduced cooling system requirements (enabling 30-40% reduction in radiator volume), increased power density (allowing more compact inverter designs), and improved cold-weather performance due to lower conduction losses [62,63].

Beyond traction inverters, SiC devices are also used in on-board chargers (OBCs) and DC-DC converters for high-performance vehicles. In OBC applications, SiC enables bidirectional power flow with efficiencies exceeding 96% across the entire power range, facilitating Vehicle-to-Grid (V2G) integration [65,91]. However, GaN devices are increasingly competing with SiC in lower-power OBC segments (typically below 11 kW) and DC-DC converter applications, where their superior switching speed and lower gate charge offer advantages in high-frequency operation [92].

GaN-based devices becomes particularly preferable over SiC counterparts in several application scenarios. For low-to-medium power OBCs (3.3–11 kW), GaN's lower switching losses at frequencies above 100 kHz enable higher power density and reduced passive component size, while maintaining competitive costs at these power levels [93]. For isolated DC-DC converters (400 V to 12/48 V), GaN's fast switching enables resonant and quasi-resonant topologies with switching frequencies exceeding 500 kHz, significantly reducing magnetic component volume [94].

Table 12 summarizes the adoption of WBG devices in electric vehicle applications by major manufacturers [95,96].

Table 12. WBG Device Adoption in Electric Vehicle Applications, data taken from [95,96].

OEM	Model	Tech	Application	Perf. Gain	Year
Tesla	Model 3/Y	SiC	Traction Inverter	+8% range	2017
BYD	Han EV	SiC	Traction + OBC	+5% efficiency	2020
Lucid	Air	SiC	900V Inverter	+10% range	2021
Hyundai	IONIQ 5	SiC	800V Charging	18 min charge	2021
Mercedes	EQS	SiC	Traction Inverter	+6% range	2022
BMW	iX	GaN	OBC	40% size red.	2022
Porsche	Taycan	SiC	800V System	270kW charge	2019
VW	ID.7	SiC	APP310 Inv.	+5% efficiency	2023

8.2. Consumer Electronics and Power Delivery

GaN transistors are commonly used in power supplies and chargers for consumer electronics like smartphones and laptops. Thanks to their ability to operate at switching frequencies exceeding 1 MHz [78,97], GaN enables the development of more compact and powerful chargers—up to three times smaller than traditional Si-based AC–DC converters. The high-frequency operation allows for a

© 2025 by the author(s). Distributed under a Creative Commons CC BY license.

Preprints.org (www.preprints.org) | NOT PEER-REVIEWED | Posted: 29 January 2026 doi:10.20944/preprints202601.2280.v1

significant reduction in passive component size: at 1 MHz, inductors and capacitors can be reduced to 10-20% of their 100 kHz equivalents [98].

GaN devices are also increasingly used in premium photovoltaic (PV) inverters where efficiency improvements of 0.5-1% translate to significant lifetime energy gains. For a typical 5 kW residential system, a 1% efficiency improvement yields approximately 400-500 kWh additional energy annually, corresponding to €50-80 in extra revenue over a 25-year lifetime [67]. Recent developments include multi-level topologies (NPC, T-type, Active Neutral Point Clamped (ANPC)) that leverage GaN's fast switching to achieve peak efficiencies of 99.2% in the 5-20 kW range [99].

9. Reliability and Practical Constraints

While WBG devices offer superior performance, successful deployment requires careful attention to specific reliability challenges for both SiC and GaN technologies [100,101]. Hereafter, a comparison between SiC and GaN devices' reliability is carried out.

9.1. SiC Technology Challenges

Despite significant progress, SiC technology faces several practical challenges requiring careful consideration in system design [102,103]:

Gate oxide reliability: The SiC/SiO_2 interface exhibits higher defect density than Si/SiO_2, leading to threshold voltage instability under bias-temperature stress. Modern devices employ nitrogen annealing and optimized oxide growth to mitigate this, achieving lifetimes exceeding 10^7 hours at rated conditions [102].

Body diode performance: The intrinsic body diode of SiC MOSFETs exhibits significant forward voltage drop (3–4 V) and associated conduction losses during dead-time intervals. Anti-parallel SiC Schottky diodes or synchronous rectification techniques address this limitation.

Short-circuit withstand time: SiC MOSFETs typically withstand short-circuit conditions for 2–5 μs, compared to 10 μs for Si IGBTs. Fast desaturation detection (<200 ns) and active gate clamping are essential protection features [104].

Cost premium: SiC devices remain 2–3× more expensive than Si equivalents on a per-amp basis, though the transition to 200 mm wafer production (operational by 2026) is expected to reduce this premium to 1.5–2× by 2028 [105].

9.2. GaN Technology Challenges

9.2.1. Dynamic On-Resistance

GaN devices can exhibit increased $R_{DS(on)}$ after blocking high voltages—a phenomenon known as dynamic on-resistance or current collapse [79,106]. This occurs due to charge trapping in the AlGaN barrier or GaN buffer layers. The magnitude of degradation can reach 2–5× the static value.

The time constants for trap filling and emission range from microseconds to seconds [107]. Mitigation strategies include operating with reduced blocking voltage margins, gate voltage optimization during off-state, using p-GaN gate technology, and selecting devices with optimized buffer designs [108].

9.2.2. Short Circuit and Overcurrent Protection

GaN HEMTs have limited short-circuit withstand time (<1 μs) compared to SiC MOSFETs (2–5 μs) and Si IGBTs (10 μs) [104]. This necessitates extremely fast protection schemes including desaturation detection with <100 ns response time, active gate clamping, and fast shutdown protocols with controlled di/dt.

© 2025 by the author(s). Distributed under a Creative Commons CC BY license.

Preprints.org (www.preprints.org) | NOT PEER-REVIEWED | Posted: 29 January 2026 doi:10.20944/preprints202601.2280.v1

9.3. Common Reliability Considerations

9.3.1. Threshold Voltage Instability

Both SiC and GaN devices experience threshold voltage shifts under bias-temperature stress [102,103]. The shift typically follows:

$$\Delta V_{th}(t) = A\log(1 + t/\tau) \tag{18}$$

where A and τ are temperature and field-dependent parameters.

Modern gate drive designs address this through negative gate bias during off-state ($V_{GS} = -2$ to -5 V for SiC), active gate charge monitoring, and temperature-compensated gate drive voltage [70].

9.3.2. Packaging and Thermal Management

Advanced packaging is critical for realizing WBG benefits [109,110]. Table 13 summarizes typical parasitic values for different packaging technologies.

Table 13. Parasitic Inductance Comparison for Different Packages, data taken from [111,112].

Package	L_{pkg} **(nH)**	L_{PCB} **(nH)**	C_{par} **(pF)**	**Max** f_{sw} **Range**
TO-247	10–15	5–10	5–10	<100 kHz
D2PAK	5–8	3–5	3–5	<500 kHz
SMD (GaN)	0.5–2	1–3	1–2	>1 MHz
Chip-scale	0.1–0.5	0.5–1	0.5–1	>5 MHz
DFN (QFN)	1–3	2–4	2–3	200–800 kHz
LGA	0.3–1	0.8–2	1–2	1–3 MHz

Key packaging requirements include low parasitic inductance (<5 nH for GaN, <10 nH for SiC), low thermal resistance (<0.3 K/W junction-to-case), Coefficient of Thermal Expansion (CTE) matching between die and substrate, and high-temperature capable material (>200°C) [113,114].

The junction temperature rise is:

$$\Delta T_j = P_{loss} \cdot (R_{th(j-c)} + R_{th(c-s)} + R_{th(s-a)}) \tag{19}$$

For transient thermal analysis [115]:

$$T_j(t) = T_{ambient} + P_{loss}\sum_{i=1}^{n} R_{th,i}\left(1 - e^{-t/\tau_i}\right) \tag{20}$$

Key developments in power packaging require both to reduce the thermal resistance and capacitance of the device, in order to allow a more effective heat removal.

10. Conclusions and Future Perspectives

Wide-bandgap and ultrawide-bandgap semiconductors represent a strategic enabling technology for global sustainability initiatives, offering revolutionary improvements in power conversion efficiency (2–5%), power density (3–5×), and thermal performance across critical applications from electric vehicles to data centers and renewable energy systems [3,8].

This comprehensive review has employed a bottom-up approach to demonstrate that the transition from silicon to WBG materials provides measurable benefits at material, device, converter, and system levels. Through detailed analysis of figures of merit, we showed that SiC and GaN offer 18–850× improvements in key performance metrics compared to silicon [24,27]. Case studies across automotive, industrial, and consumer sectors quantified economic benefits including payback periods of 1.5–2.5 years for most applications.

Emerging device technologies are extending WBG capabilities into new application domains. Vertical GaN devices, with demonstrations of 1.2 kV+ blocking voltage and 50 A current capability, are poised to challenge SiC in medium-voltage applications during the 2027–2030 timeframe [54,55].

© 2025 by the author(s). Distributed under a Creative Commons CC BY license.

Preprints.org (www.preprints.org) | NOT PEER-REVIEWED | Posted: 29 January 2026 doi:10.20944/preprints202601.2280.v1

Monolithic bidirectional GaN switches enable revolutionary single-stage power conversion topologies, eliminating DC-link capacitors and achieving up to 50% size reductions in EV chargers and solar inverters [59,61]. The comprehensive topology comparison presented in this review provides design engineers with practical guidelines for optimal device selection across application domains.

The emergence of UWBG materials represents the next frontier in power semiconductor development. β-Ga_2O_3 offers exceptional BFOM (3444× silicon) and cost-effective melt-growth production, with 4-inch wafers commercially available and commercialization projected for 2027–2030. AlN has demonstrated record electric field capability (7.3 MV/cm) through innovative distributed polarization doping, with European consortia establishing complete value chains and commercialization expected in the 2030s. Diamond, the ultimate semiconductor material with BFOM 50,000× silicon, has achieved breakthrough demonstrations including 4.6 kV devices and the first n-channel MOSFETs, with Japanese industry targeting vehicle applications by the 2030s. Cubic boron nitride (c-BN), with the highest bandgap (6.4 eV) among practical semiconductors and superior doping flexibility compared to diamond, offers potential for ultra-high-voltage (>10 kV) applications, though manufacturing scalability remains a key challenge with commercialization projected beyond 2035 [39,41].

However, successful deployment requires addressing specific challenges including dynamic on-resistance degradation in GaN devices [79], threshold voltage instability in both SiC and GaN [102,103], electromagnetic interference from fast switching transitions [116], and limited short-circuit withstand capability [104]. Advanced gate drive designs optimized for each technology, as detailed in Table 9, along with optimized PCB layouts and sophisticated control algorithms provide effective mitigation strategies.

Supply chain considerations have become increasingly important, with geopolitical tensions creating parallel technological ecosystems and highlighting the need for diversified sourcing strategies. The concentration of gallium production in China and the strategic importance of WBG semiconductors for electric vehicles, renewable energy, and defense applications underscore the need for continued investment in domestic manufacturing capabilities.

Future research directions include development of standardized reliability testing protocols for WBG devices, integration of on-chip protection and diagnostic functions, advanced packaging solutions for higher power densities [113], AI-based optimization of converter control and EMI mitigation, and continued development of UWBG materials toward commercial viability.

As manufacturing yields improve and costs decrease—with approximately 20% year-over-year cost reductions observed over the past five years [89]—WBG adoption will continue to accelerate. The emergence of 200 mm (8-inch) SiC wafer production and continued scaling of GaN-on-Si technology will further improve economics. Within the next decade, WBG devices are expected to dominate medium and high-power applications, while UWBG materials will enable the next generation of ultra-high-voltage systems essential for grid infrastructure, space applications, and extreme environments.

Author Contributions: Conceptualization, G.G. and G.V.; methodology, G.G.; investigation, G.G. and G.C.G.; writing—original draft preparation, G.G.; writing—review and editing, G.V., G.C.G., A.S. and G.L.; supervision, G.V. and G.L. All authors have read and agreed to the published version of the manuscript.

Funding: This work has been carried out in the framework of the European Project GaN4AP (Gallium Nitride for Advanced Power Applications). The project has received funding from the Electronic Component Systems for European Leadership Joint Undertaking (ECSEL JU), under grant agreement No.101007310. This Joint Undertaking receives support from the European Union's Horizon 2020 research and innovation programme, and from Italy, France, Poland, Czech Republic, Netherlands.

Institutional Review Board Statement: Not applicable.

Informed Consent Statement: Not applicable.

Data Availability Statement: No new data were created or analyzed in this study. Data sharing is not applicable to this article.

© 2025 by the author(s). Distributed under a Creative Commons CC BY license.

Preprints.org (www.preprints.org) | NOT PEER-REVIEWED | Posted: 29 January 2026

doi:10.20944/preprints202601.2280.v1

Conflicts of Interest: The authors declare no conflicts of interest.

© 2025 by the author(s). Distributed under a Creative Commons CC BY license.

Preprints.org (www.preprints.org) | NOT PEER-REVIEWED | Posted: 29 January 2026
doi:10.20944/preprints202601.2280.v1

Abbreviations

The following abbreviations are used in this manuscript:

2DEG	Two-Dimensional Electron Gas	AlN	Aluminum Nitride	ANPC	Active Neutral Point Clamped
BDS	Bidirectional Switch	BFOM	Baliga Figure of Merit	BHFFOM	Baliga High-Frequency FOM
BJT	Bipolar Junction Transistor	CAGR	Compound Annual Growth Rate	CAVET	Current Aperture Vertical Electron Trans.
c-BN	Cubic Boron Nitride	CCM	Continuous Conduction Mode	CHFFOM	Combined High-Freq. FOM
CMTI	Common-Mode Transient Immun.	CSI	Current Source Inverter	CTE	Coeff. of Thermal Expansion
CVD	Chemical Vapor Deposition	CZ	Czochralski	DAB	Dual Active Bridge
DFN	Dual Flat No-lead	D-mode	Depletion Mode	DOE	Department of Energy
DPD	Distributed Polarization Doping	EFG	Edge-defined Film-fed Growth	EMI	Electromagnetic Interference
E-mode	Enhancement Mode	ESR	Equivalent Series Resistance	ETRI	Korea Elec. & Telecom. Res. Inst.
EV	Electric Vehicle	FET	Field-Effect Transistor	FOM	Figure of Merit
FZ	Floating Zone	GaN	Gallium Nitride	h-BN	hexagonal Boron Nitride
HEMT	High Electron Mobility Trans.	HERIC	Highly Eff. & Reliable Inv. Concept	HPHT	High-Pressure High-Temp.
HVDC	High-Voltage Direct Current	IEDM	Intl. Electron Devices Meeting	IGBT	Insulated-Gate Bipolar Trans.
JAXA	Japan Aerospace Expl. Agency	JFET	Junction Field-Effect Trans.	JFOM	Johnson's Figure of Merit
KFOM	Keyes' Figure of Merit	KPI	Key Performance Indicator	LGA	Land Grid Array
MOSFET	Metal-Oxide-Semicond. FET	NIMS	Natl. Inst. for Materials Sci.	NPC	Neutral Point Clamped
OBC	On-Board Charger	OEM	Original Equip. Manufacturer	PCB	Printed Circuit Board
PFC	Power Factor Correction	PLA	Pulsed Laser Annealing	PRISMA	Pref. Rep. Items for Syst. Rev.
PSU	Power Supply Unit	PV	Photovoltaic	PWM	Pulse Width Modulation
QFN	Quad Flat No-lead	RF	Radio Frequency	SBD	Schottky Barrier Diode
SiC	Silicon Carbide	SMD	Surface Mount Device	TFOM	Thermal Figure of Merit
THD	Total Harmonic Distortion	TRL	Technology Readiness Level	UVLO	Under-Voltage Lockout
UWBG	Ultrawide-Bandgap	V2G	Vehicle-to-Grid	VFD	Variable Frequency Drive
VSI	Voltage Source Inverter	WBG	Wide-Bandgap	ZVS	Zero Voltage Switching

© 2025 by the author(s). Distributed under a Creative Commons CC BY license.

Preprints.org (www.preprints.org) | NOT PEER-REVIEWED | Posted: 29 January 2026
doi:10.20944/preprints202601.2280.v1

References

1. International Energy Agency. CO2 Emissions in 2023. Available online: https://www.iea.org/reports/co2-emissions-in-2023 (accessed on 27 January 2026), 2024.
2. Liu, Z.; Deng, Z.; Davis, S.J.; Ciais, P. Global Carbon Emissions in 2023. *Nature Reviews Earth and Environment* **2024**, *5*, 253–254. https://doi.org/10.1038/s43017-024-00532-2.
3. Tsao, J.Y.; et al. Ultrawide-Bandgap Semiconductors: Research Opportunities and Challenges. *Advanced Electronic Materials* **2018**, *4*, 1600501. https://doi.org/10.1002/aelm.201600501.
4. Millán, J.; Godignon, P.; Perpiñà, X.; Pérez-Tomás, A.; Rebollo, J. A Survey of Wide Bandgap Power Semiconductor Devices. *IEEE Transactions on Power Electronics* **2014**, *29*, 2155–2163. https://doi.org/10.1109/TPEL.2013.2268900.
5. Baliga, B.J. *Fundamentals of Power Semiconductor Devices*; Springer: New York, NY, USA, 2008. https://doi.org/10.1007/978-0-387-47314-7.
6. Vitale, G. Power Converters for Green Hydrogen: State of the Art and Perspectives. *Electronics* **2024**, *13*, 4565. https://doi.org/10.3390/electronics13224565.
7. Guilbert, D.; Vitale, G. Hydrogen as a Clean and Sustainable Energy Vector for Global Transition from Fossil-Based to Zero-Carbon. *Clean Technologies* **2021**, *3*, 881–909. https://doi.org/10.3390/cleantechnol3040051.
8. Buffolo, M.; et al. Review of Reliability and Failure Analysis of Wide and Ultrawide Bandgap Semiconductor Devices. *Journal of Physics D: Applied Physics* **2024**, *57*, 013001. https://doi.org/10.1088/1361-6463/acf30b.
9. Vitale, G. Energy Saving by Power Electronics: Towards a New Concept of Renewable Source. *Renewable Energy and Power Quality Journal* **2016**, *4*, 160001–160010. https://doi.org/10.24084/repqj14.001.
10. Google. Data Center Efficiency. Available online: https://sustainability.google/operating-sustainably/net-zero-carbon/ (accessed on 27 January 2026), 2023.
11. Tesla, Inc.. 2023 Impact Report. Available online: https://www.tesla.com/ns_videos/2023-tesla-impact-report.pdf (accessed on 27 January 2026), 2023.
12. Kim, T.; et al. Silicon Carbide Inverter Performance Analysis for Electric Vehicles. *IEEE Transactions on Industry Applications* **2019**, *55*, 5620–5630. https://doi.org/10.1109/TIA.2019.2927669.
13. Page, M.J.; McKenzie, J.E.; Bossuyt, P.M.; Boutron, I.; Hoffmann, T.C.; Mulrow, C.D.; Shamseer, L.; Tetzlaff, J.M.; Akl, E.A.; Brennan, S.E.; et al. The PRISMA 2020 Statement: An Updated Guideline for Reporting Systematic Reviews. *BMJ* **2021**, *372*, n71. https://doi.org/10.1136/bmj.n71.
14. Rafin, S.S.H.; Ahmed, R.; et al. Power Electronics Revolutionized: A Comprehensive Analysis of Emerging Wide and Ultrawide Bandgap Devices. *Micromachines* **2023**, *14*, 2045. https://doi.org/10.3390/mi14112045.
15. Chow, T.P.; et al. Wide-Bandgap Semiconductors and Power Electronics as Pathways to Carbon Neutrality. *Nature Reviews Electrical Engineering* **2025**, *2*, 1–15. https://doi.org/10.1038/s44287-024-00135-5.
16. Kumar, V.; et al. Wide Bandgap Semiconductor Devices for Power Electronics. *Semiconductor Science and Technology* **2022**, *37*, 043001. https://doi.org/10.1088/1361-6641/ac43e9.
17. She, X.; Huang, A.Q.; Lucia, O.; Ozpineci, B. Review of Silicon Carbide Power Devices and Their Applications. *IEEE Transactions on Industrial Electronics* **2014**, *61*, 5920–5935. https://doi.org/10.1109/TIE.2014.2314065.
18. Wu, X.; Zhang, L.; You, H.; Zhang, S.; Nikolov, D.; Cui, Q. EMC-Friendly Gate Driver Design in GaN-Based DC-DC Converters for Automotive Electronics: A Review. *Electronics* **2026**, *15*, 283. https://doi.org/10.3390/electronics15020283.
19. Bourzac, K. The New, New Transistor: AlN Diodes Withstand Electric Fields Twice as High as SiC or GaN. Available online: https://spectrum.ieee.org/aluminum-nitride (accessed on 27 January 2026), 2024.
20. Hobart, K.D.; et al. Record Breakdown Voltage Diamond Schottky Barrier Diodes. *Applied Physics Letters* **2024**, *124*, 052105. https://doi.org/10.1063/5.0186509.
21. National Institute for Materials Science. First n-Channel Diamond MOSFET Demonstration. *Functional Diamond* **2024**, *4*, 1–8. https://doi.org/10.1080/26941112.2024.2308622.
22. Ambacher, O.; et al. Two-Dimensional Electron Gases Induced by Spontaneous and Piezoelectric Polarization Charges. *Journal of Applied Physics* **1999**, *85*, 3222–3233. https://doi.org/10.1063/1.369664.
23. Razeeb, K.M.; et al. Present and Future Thermal Interface Materials for Electronic Devices. *International Materials Reviews* **2018**, *63*, 1–21. https://doi.org/10.1080/09506608.2017.1296605.
24. Baliga, B.J. Power Semiconductor Device Figure of Merit for High-Frequency Applications. *IEEE Electron Device Letters* **1989**, *10*, 455–457. https://doi.org/10.1109/55.43098.
25. Johnson, E.O. Physical Limitations on Frequency and Power Parameters of Transistors. *RCA Review* **1965**, *26*, 163–177.

© 2025 by the author(s). Distributed under a Creative Commons CC BY license.

Preprints.org (www.preprints.org) | NOT PEER-REVIEWED | Posted: 29 January 2026

doi:10.20944/preprints202601.2280.v1

26. Keyes, R.W. Figure of Merit for Semiconductors for High-Speed Switches. *Proceedings of the IEEE* **1972**, *60*, 225. https://doi.org/10.1109/PROC.1972.8593.
27. Hudgins, J.L.; Simin, G.S.; Santi, E.; Khan, M.A. An Assessment of Wide Bandgap Semiconductors for Power Devices. *IEEE Transactions on Power Electronics* **2003**, *18*, 907–914. https://doi.org/10.1109/TPEL.2003.810840.
28. Baliga, B.J. Trends in Power Semiconductor Devices. *IEEE Transactions on Electron Devices* **1996**, *43*, 1717–1731. https://doi.org/10.1109/16.536819.
29. Sharma, R.; Chiriac, M.M.; et al. Thermal Management of GaN Power Devices: A Review. *IEEE Journal of Emerging and Selected Topics in Power Electronics* **2016**, *4*, 99–108. https://doi.org/10.1109/JESTPE.2015.2503220.
30. Higashiwaki, M.; Sasaki, K. Gallium Oxide (β-Ga_2O_3) Power Devices: Progress and Prospects. *Applied Physics Letters* **2022**, *120*, 110503. https://doi.org/10.1063/5.0086062.
31. Sun, J.; et al. Recent Progress in β-Ga_2O_3 Power Electronics. *APL Materials* **2024**, *12*, 030901. https://doi.org/10.1063/5.0191343.
32. Korea Electronics and Telecommunications Research Institute. 3 kV-Class β-Ga_2O_3 MOSFETs Demonstration. *IEEE Electron Device Letters* **2024**, *45*, 1001–1004. https://doi.org/10.1109/LED.2024.3383726.
33. Wong, M.H.; et al. β-Ga_2O_3 Heterojunction Devices for Power Electronics. *Journal of Applied Physics* **2024**, *135*, 011101. https://doi.org/10.1063/5.0179714.
34. Faber, H.; et al. Aluminum Nitride Power Devices: Progress and Challenges. *Advanced Materials* **2024**, *36*, 2308096. https://doi.org/10.1002/adma.202308096.
35. Fraunhofer IISB. AlN-Based Power Devices Value Chain Demonstration. Available online: https://www.iisb.fraunhofer.de/en/research_areas/energy_electronics.html (accessed on 27 January 2026), 2024.
36. Crystal IS. 100mm Single-Crystal AlN Substrates. Available online: https://www.crystal-is.com/products/aln-substrates/ (accessed on 27 January 2026), 2024.
37. Donato, N.; et al. Diamond Power Devices: State of the Art and Prospects. *Materials Science in Semiconductor Processing* **2024**, *167*, 107789. https://doi.org/10.1016/j.mssp.2023.107789.
38. Electropages. Japanese Diamond Semiconductor Development. Available online: https://www.electropages.com/blog/2024/03/japanese-diamond-semiconductor-development (accessed on 27 January 2026), 2024.
39. Narayan, J. Recent Progress in Cubic Boron Nitride for High-Power Electronics. *APL Materials* **2021**, *9*, 050401. https://doi.org/10.1063/5.0052112.
40. Minnich, A.J. Doping and Electrical Properties of Cubic Boron Nitride: A Critical Review. *Thin Solid Films* **2024**, *785*, 140102. https://doi.org/10.1016/j.tsf.2023.140102.
41. Haque, A.; Taqy, S.; Narayan, J. Recent Progress in Cubic Boron Nitride (c-BN) Fabrication by Pulsed Laser Annealing for Optoelectronic Applications. *Journal of Electronic Materials* **2024**, *53*, 4308–4340. https://doi.org/10.1007/s11664-024-11172-8.
42. Haque, A.; Narayan, J. Tunable n-Type Conductivity and Transport Properties of Cubic Boron Nitride via Carbon Doping. *ACS Applied Electronic Materials* **2021**, *3*, 1406–1417. https://doi.org/10.1021/acsaelm.0c01094.
43. Pimputkar, S. Development of Cubic Boron Nitride Semiconductors. Lehigh University Research, NSF CAREER Grant. Available online: https://engineering.lehigh.edu/faculty/siddha-pimputkar (accessed on 27 January 2026), 2024.
44. Narayan, J.; Bhaumik, A. Direct Conversion of h-BN into c-BN and Formation of Epitaxial c-BN/Diamond Heterostructures. *Journal of Applied Physics* **2016**, *119*, 185302. https://doi.org/10.1063/1.4948688.
45. U.S. Department of Energy. Development of Cubic Boron Nitride (c-BN) Ultrawide Bandgap Semiconductors. Texas Tech University Project CX-028884. Available online: https://www.energy.gov/ (accessed on 27 January 2026), 2024.
46. Mullen, J.T.; et al. Electronic Properties of c-BN/Diamond Heterostructures for High-Frequency High-Power Applications. *Diamond and Related Materials* **2024**, *143*, 110920. https://doi.org/10.1016/j.diamond.2024.110920.
47. Jones, E.A.; Wang, F.F.; Costinett, D. Review of Commercial GaN Power Devices and GaN-Based Converter Design Challenges. *IEEE Journal of Emerging and Selected Topics in Power Electronics* **2016**, *4*, 707–719. https://doi.org/10.1109/JESTPE.2016.2582685.
48. Lidow, A.; Strydom, J.; de Rooij, M.; Reusch, D. *GaN Transistors for Efficient Power Conversion*; John Wiley & Sons: Hoboken, NJ, USA, 2014. https://doi.org/10.1002/9781118844779.
49. Kimoto, T.; Cooper, J.A. *Fundamentals of Silicon Carbide Technology*; Wiley-IEEE Press: Hoboken, NJ, USA, 2014. https://doi.org/10.1002/9781118313534.

© 2025 by the author(s). Distributed under a Creative Commons CC BY license.

Preprints.org (www.preprints.org) | NOT PEER-REVIEWED | Posted: 29 January 2026 doi:10.20944/preprints202601.2280.v1

50. Nakamura, T.; et al. High Performance SiC Trench Devices with Ultra-Low Ron. In Proceedings of the Proceedings of the IEEE International Electron Devices Meeting (IEDM), 2011, pp. 26.5.1–26.5.3. https://doi.org/10.1109/IEDM.2011.6131619.
51. Chen, K.J.; et al. GaN-on-Si Power Technology: Devices and Applications. *IEEE Transactions on Electron Devices* **2017**, *64*, 779–795. https://doi.org/10.1109/TED.2017.2657579.
52. Uemoto, Y.; et al. Gate Injection Transistor (GIT)—A Normally-Off AlGaN/GaN Power Transistor. *IEEE Transactions on Electron Devices* **2007**, *54*, 3393–3399. https://doi.org/10.1109/TED.2007.908601.
53. Chen, J.; et al. Reliability Assessment of E-mode GaN HEMTs for Power Applications. *Microelectronics Reliability* **2024**, *152*, 115325. https://doi.org/10.1016/j.microrel.2023.115325.
54. Shenoy, P.M.; et al. Vertical GaN MOSFET Power Devices. *Micromachines* **2023**, *14*, 1937. https://doi.org/10.3390/mi14101937.
55. onsemi. Onsemi Unveils Vertical GaN Semiconductors: A Breakthrough for AI and Electrification. Available online: https://www.onsemi.com/company/news-media/press-announcements/en/onsemi-unveils-vertical-gan-semiconductors (accessed on 27 January 2026), 2024.
56. Toyoda Gosei. 50-Amp High-Voltage Vertical GaN Power Semiconductors. In Proceedings of the Proceedings of the PCIM Europe, 2024, pp. 1–6.
57. Nie, H.; et al. 1.2 kV Vertical GaN Fin-Channel JFET: Comprehensive Evaluation in Converter Applications. *IEEE Transactions on Power Electronics* **2024**, *39*, 6120–6132. https://doi.org/10.1109/TPEL.2024.3352303.
58. Posthuma, N.E.; et al. Vertical GaN Devices: Process and Reliability. *Microelectronics Reliability* **2021**, *125*, 114342. https://doi.org/10.1016/j.microrel.2021.114342.
59. Infineon Technologies. Revolutionizing Power Electronics: GaN Bidirectional Switches. Available online: https://www.infineon.com/cms/en/product/power/gallium-nitride-gan/gan-bidirectional-switches/ (accessed on 27 January 2026), 2024.
60. Infineon Technologies. CoolGaN Bidirectional Switch and Smart Sense Products. Available online: https://www.infineon.com/cms/en/product/power/gallium-nitride-gan/gan-bidirectional-switches/ (accessed on 27 January 2026), 2024.
61. Navitas Semiconductor. Navitas Drives a Paradigm Shift in Power with Single-Stage BDS Converters. Available online: https://navitassemi.com/products/ganbds/ (accessed on 27 January 2026), 2025.
62. Wang, F.; Zhang, Z. Overview of Wide Bandgap Devices and Their Applications in Automotive Systems. *IEEE Journal of Emerging and Selected Topics in Power Electronics* **2021**, *9*, 6572–6588. https://doi.org/10.1109/JESTPE.2021.3078666.
63. Biela, J.; Schweizer, M.; Waffler, S.; Kolar, J.W. SiC versus Si—Evaluation of Potentials for Performance Improvement in Automotive Applications. *IEEE Transactions on Industrial Electronics* **2011**, *58*, 2872–2882. https://doi.org/10.1109/TIE.2010.2072896.
64. Johnson, P.M.; et al. SiC-Based Traction Inverter Design for Electric Vehicles. *IEEE Transactions on Transportation Electrification* **2024**, *10*, 245–258. https://doi.org/10.1109/TTE.2023.3267890.
65. Whitaker, B.; et al. A High-Density, High-Efficiency, Isolated On-Board Vehicle Battery Charger Utilizing SiC Power Devices. *IEEE Transactions on Power Electronics* **2014**, *29*, 2606–2617. https://doi.org/10.1109/TPEL.2013.2279950.
66. Azurza, J.; et al. Vienna Rectifier-Based DC Fast Charging Station. *IEEE Transactions on Industrial Electronics* **2019**, *66*, 6175–6185. https://doi.org/10.1109/TIE.2018.2870391.
67. Karanayil, B.; et al. Review of Solar PV Inverter Topologies and Technologies. *Renewable and Sustainable Energy Reviews* **2021**, *150*, 111459. https://doi.org/10.1016/j.rser.2021.111459.
68. Gu, Y.; et al. A Symmetric T-Type Inverter for Solar Photovoltaic Applications. *IEEE Transactions on Industrial Electronics* **2015**, *62*, 2209–2219. https://doi.org/10.1109/TIE.2014.2345341.
69. Reusch, D.; Strydom, J. Understanding the Effect of PCB Layout on Circuit Performance. *IEEE Transactions on Power Electronics* **2014**, *29*, 2008–2018. https://doi.org/10.1109/TPEL.2013.2266103.
70. Dalal, D.N.; et al. Gate Driver Design Optimization for WBG Power Devices. *IEEE Transactions on Power Electronics* **2018**, *33*, 7885–7897. https://doi.org/10.1109/TPEL.2017.2772841.
71. Mu, M.; et al. High-Frequency Switching Loss Analysis of GaN-Based Buck Converter. *IEEE Transactions on Power Electronics* **2013**, *28*, 4510–4517. https://doi.org/10.1109/TPEL.2012.2233759.
72. Erickson, R.W.; Maksimović, D. *Fundamentals of Power Electronics*, 2nd ed.; Springer: Boston, MA, USA, 2001. https://doi.org/10.1007/b100747.
73. Barroso, J.; et al. Interleaved Buck Converter for High-Power Applications. *IEEE Transactions on Power Electronics* **2013**, *28*, 5633–5643. https://doi.org/10.1109/TPEL.2013.2248750.

© 2025 by the author(s). Distributed under a Creative Commons CC BY license.

Preprints.org (www.preprints.org) | NOT PEER-REVIEWED | Posted: 29 January 2026 doi:10.20944/preprints202601.2280.v1

74. Li, W.; et al. Precise Phase Current Sharing for Interleaved Converters. *IEEE Transactions on Power Electronics* **2017**, *32*, 650–661. https://doi.org/10.1109/TPEL.2016.2535365.
75. De Doncker, R.W.; Divan, D.M.; Kheraluwala, M.H. A Three-Phase Soft-Switched High-Power-Density DC/DC Converter. *IEEE Transactions on Industry Applications* **1991**, *27*, 63–73. https://doi.org/10.1109/28.67533.
76. Kheraluwala, M.H.; Gascoigne, R.W.; Divan, D.M.; Baumann, E.D. Performance Characterization of a High-Power Dual Active Bridge DC-DC Converter. *IEEE Transactions on Industry Applications* **1992**, *28*, 1294–1301. https://doi.org/10.1109/28.175280.
77. Everts, J. Design and Optimization of an Efficient (96.1%) and Compact DAB Converter. *IEEE Transactions on Power Electronics* **2014**, *29*, 3919–3929. https://doi.org/10.1109/TPEL.2013.2282318.
78. Rodriguez, J.; et al. High-Frequency PWM in Multilevel Converter Applications. *IEEE Transactions on Industrial Electronics* **2014**, *61*, 4182–4191. https://doi.org/10.1109/TIE.2013.2286565.
79. Badawi, N.; et al. Investigation of the Dynamic On-State Resistance of GaN HEMTs. *IEEE Transactions on Power Electronics* **2016**, *31*, 5781–5793. https://doi.org/10.1109/TPEL.2015.2489560.
80. Power Electronics News. Gallium Nitride Monolithic Bidirectional Switches. Available online: https://www.powerelectronicsnews.com/gallium-nitride-monolithic-bidirectional-switches/ (accessed on 27 January 2026), 2025.
81. Paredes, A.; et al. Gate Driver Design for WBG Power Devices. *Electronics* **2021**, *10*, 1273. https://doi.org/10.3390/electronics10111273.
82. onsemi. SiC MOSFET Gate Driver Design Guide. Application Note AND9956/D. Available online: https://www.onsemi.com/pub/Collateral/AND9956-D.PDF (accessed on 27 January 2026), 2021.
83. Future Electronics. Gate Driver Solutions for WBG Semiconductors. Technical Report. Available online: https://www.futureelectronics.com/resources/gate-drivers (accessed on 27 January 2026), 2022.
84. Navitas Semiconductor. GaNSafe Power ICs. Available online: https://navitassemi.com/products/gansafe/ (accessed on 27 January 2026), 2024.
85. Kolar, J.W.; et al. Optimization of Ultra-Compact Power Converters. *CPSS Transactions on Power Electronics and Applications* **2016**, *1*, 14–28. https://doi.org/10.24295/CPSSTPEA.2016.00002.
86. Hurley, W.G.; Wölfle, W.H. *Transformers and Inductors for Power Electronics*; Wiley: Chichester, UK, 2013. https://doi.org/10.1002/9781118544648.
87. Sullivan, C.R. Overview of Core Materials for Inductors. In Proceedings of the Proceedings of the IEEE Applied Power Electronics Conference, 2012, pp. 1–12. https://doi.org/10.1109/APEC.2012.6165803.
88. Chen, W.; et al. Integrated Magnetic Design for High-Frequency Converters. *IEEE Transactions on Power Electronics* **2009**, *24*, 1851–1862. https://doi.org/10.1109/TPEL.2009.2016662.
89. Wolfspeed. 200mm SiC Wafer Production Announcement. Available online: https://www.wolfspeed.com/company/news-events/wolfspeed-200mm-sic-wafer (accessed on 27 January 2026), 2023.
90. Lidow, A. Comparing GaN and SiC: Device Performance and Applications. *Power Electronics Europe* **2019**.
91. Musavi, F.; Eberle, W. Overview of Wireless Power Transfer Technologies for Electric Vehicle Battery Charging. *IET Power Electronics* **2014**, *7*, 60–66. https://doi.org/10.1049/iet-pel.2013.0047.
92. Huang, A.Q.; et al. Review of GaN Power Devices and Applications. *CPSS Transactions on Power Electronics and Applications* **2020**, *5*, 4–14. https://doi.org/10.24295/CPSSTPEA.2020.00002.
93. Lee, W.; et al. Comparative Study of GaN and SiC Based On-Board Chargers for Electric Vehicles. *IEEE Transactions on Power Electronics* **2021**, *36*, 11580–11593. https://doi.org/10.1109/TPEL.2021.3071364.
94. Han, D.; et al. High-Frequency GaN-Based Isolated DC-DC Converter for Electric Vehicle Applications. *IEEE Transactions on Industry Applications* **2018**, *54*, 3558–3567. https://doi.org/10.1109/TIA.2018.2823662.
95. IDTechEx. Power Electronics for Electric Vehicles 2024-2034. Available online: https://www.idtechex.com/en/research-report/power-electronics-for-electric-vehicles-2024-2034/955 (accessed on 27 January 2026), 2024.
96. IDTechEx. Emerging Power Electronics Technologies. Available online: https://www.idtechex.com/en/research/power-electronics (accessed on 27 January 2026), 2024.
97. Huang, X.; et al. Analytical Loss Model of High Voltage GaN HEMT in Cascode Configuration. *IEEE Transactions on Power Electronics* **2017**, *32*, 2455–2469. https://doi.org/10.1109/TPEL.2016.2567299.
98. Chen, W.; et al. Design Optimization of GaN-Based High-Density USB-PD Charger. *IEEE Transactions on Power Electronics* **2017**, *32*, 7618–7632. https://doi.org/10.1109/TPEL.2016.2639058.
99. Zhao, H.; et al. Multilevel GaN-Based Inverter for Photovoltaic Applications. *IEEE Transactions on Industrial Electronics* **2020**, *67*, 6825–6836. https://doi.org/10.1109/TIE.2019.2939991.

© 2025 by the author(s). Distributed under a Creative Commons CC BY license.

Preprints.org (www.preprints.org) | NOT PEER-REVIEWED | Posted: 29 January 2026 doi:10.20944/preprints202601.2280.v1

100. Ciappa, M. Selected Failure Mechanisms of Modern Power Modules. *Microelectronics Reliability* **2002**, *42*, 653–667. https://doi.org/10.1016/S0026-2714(02)00042-2.
101. Wang, H.; et al. Reliability of Capacitors for DC-Link Applications. *IEEE Transactions on Industry Applications* **2012**, *48*, 1662–1670. https://doi.org/10.1109/TIA.2012.2210012.
102. Lelis, A.J.; et al. Basic Mechanisms of Threshold Voltage Instability in SiC MOSFETs. *IEEE Transactions on Electron Devices* **2014**, *62*, 316–323. https://doi.org/10.1109/TED.2014.2356172.
103. Meneghini, M.; et al. Charge Trapping in GaN Power HEMTs. *Microelectronics Reliability* **2021**, *127*, 114418. https://doi.org/10.1016/j.microrel.2021.114418.
104. Fabre, J.; et al. Robustness of SiC MOSFETs Under Short-Circuit Conditions. *Microelectronics Reliability* **2018**, *88–90*, 891–895. https://doi.org/10.1016/j.microrel.2018.07.072.
105. Atreg. WBG Semiconductor Market Trends 2025. Available online: https://atreg.com/insights/wide-bandgap-semiconductors/ (accessed on 27 January 2026), 2025.
106. Lei, J.; et al. Precise Measurement of Dynamic On-Resistance in GaN Devices. *IEEE Transactions on Industrial Electronics* **2019**, *66*, 9270–9280. https://doi.org/10.1109/TIE.2019.2896289.
107. Rossetto, I.; et al. Evidence of Current Collapse in GaN HEMTs. *Microelectronics Reliability* **2016**, *64*, 547–553. https://doi.org/10.1016/j.microrel.2016.07.045.
108. Guo, A.; del Alamo, J.A. Understanding Dynamic On-Resistance in GaN HEMTs. *IEEE Transactions on Electron Devices* **2017**, *64*, 2042–2048. https://doi.org/10.1109/TED.2017.2686840.
109. Chen, C.; et al. Flexible PCB Integration for WBG Power Modules. *IEEE Transactions on Components, Packaging and Manufacturing Technology* **2024**, *14*, 285–294. https://doi.org/10.1109/TCPMT.2024.3356789.
110. Ma, C.T.; et al. Low-Inductance Package Design for GaN Power Devices. *IEEE Transactions on Power Electronics* **2022**, *37*, 5891–5903. https://doi.org/10.1109/TPEL.2021.3134647.
111. Reusch, D.; Strydom, J. Understanding Parasitic Effects in GaN-Based Power Stages. In Proceedings of the Proceedings of the IEEE Applied Power Electronics Conference, 2014, pp. 2914–2921. https://doi.org/10.1109/APEC.2014.6803732.
112. Ma, K.; et al. Review of Power Module Packaging Technologies. *IEEE Transactions on Power Electronics* **2022**, *37*, 9527–9542. https://doi.org/10.1109/TPEL.2022.3161886.
113. Tiwari, S.; et al. 3D Packaging Technologies for WBG Power Devices. *IEEE Transactions on Components, Packaging and Manufacturing Technology* **2019**, *9*, 2416–2425. https://doi.org/10.1109/TCPMT.2019.2945765.
114. Schulz, M. Thermal Management of WBG Power Semiconductors. *Microelectronics Reliability* **2016**, *64*, 427–431. https://doi.org/10.1016/j.microrel.2016.07.099.
115. Schweitzer, D. Transient Thermal Analysis of Power Devices. *Microelectronics Reliability* **2017**, *76–77*, 36–42. https://doi.org/10.1016/j.microrel.2017.06.042.
116. Li, Y.; et al. A Survey on EMI Issues in WBG Power Converters. *IEEE Transactions on Electromagnetic Compatibility* **2023**, *65*, 345–358. https://doi.org/10.1109/TEMC.2022.3228956.

Disclaimer/Publisher's Note: The statements, opinions and data contained in all publications are solely those of the individual author(s) and contributor(s) and not of MDPI and/or the editor(s). MDPI and/or the editor(s) disclaim responsibility for any injury to people or property resulting from any ideas, methods, instructions or products referred to in the content.

© 2025 by the author(s). Distributed under a Creative Commons CC BY license.